Cross faults in extensional settings: Stress triggering, displacement localization, and implications for the origin of blunt troughs at Valles Marineris, Mars

Scott J. Wilkins[1] and Richard A. Schultz

Geomechanics-Rock Fracture Group, Department of Geological Sciences, University of Nevada, Reno, Nevada, USA

Received 9 August 2002; revised 11 December 2002; accepted 25 February 2003; published 19 June 2003.

[1] Motivated by conflicting interpretations concerning the origin of blunt terminations of troughs at Valles Marineris, Mars, we investigate the reactivation of preexisting cross faults in response to stress changes associated with slippage along a major, basin-bounding normal fault (i.e., border fault). Coulomb stress changes indicate that cross fault reactivation is possible in both the footwalls and hanging walls of border faults, although this is dependent on the distance between the border and cross faults. Cross faults accommodate dip-slip normal motion for most border fault geometries and conditions we tested, but strike-slip motions are predicted when preexisting cross faults are vertical. Furthermore, although lateral extensions of the border fault (LEBFs) may nucleate within cross fault footwalls at all stages of border fault development, they are favored to develop when border faults and cross fault tip lines are proximal. Observations from the Valles Marineris extensional province, Mars, are consistent with (1) normal displacements along cross faults, (2) numerous examples of pit-chains, interpreted to represent surface expressions of lateral extensions to the border fault (LEBF), (3) the lack of well-developed cross faults in the footwall of border faults, and (4) the inference that tapered trough ends formed in areas that lacked cross faults prior to the main phase of extension at Valles Marineris. We suggest a new sequence of deformation that accounts for the formation of blunt-trough terminations during the major phase of Valles Marineris extension: coeval and locally bidirectional extension, that results from local stress field changes associated with border fault growth in a dominantly unidirectional remote (extensional) strain field. By implication, many of the irregular closed troughs such as Hebes Chasma are better interpreted as grabens rather than collapse depressions. *INDEX TERMS:* 6225 Planetology: Solar System Objects: Mars; 8010 Structural Geology: Fractures and faults; 8020 Structural Geology: Mechanics; 8109 Tectonophysics: Continental tectonics—extensional (0905); 8164 Tectonophysics: Stresses—crust and lithosphere; *KEYWORDS:* Cross faults, release faults, stress triggering, Valles Marineris, Hebes Chasma, rift mechanics

Citation: Wilkins, S. J., and R. A. Schultz, Cross faults in extensional settings: Stress triggering, displacement localization, and implications for the origin of blunt troughs at Valles Marineris, Mars, *J. Geophys. Res.*, *108*(E6), 5056, doi:10.1029/2002JE001968, 2003.

1. Introduction

[2] Fault slip causes changes in the ambient stress field that can both stimulate and impede earthquakes in regions near the rupture patch [e.g., *Das and Scholz*, 1981; *Hudnut et al.*, 1989; *King et al.*, 1994; *Freed and Lin*, 1998; *Gomberg et al.*, 1998; *Harris*, 1998; *Harris and Simpson*, 1998; *Toda et al.*, 1998; *Stein*, 1999; *Ziv and Rubin*, 2000]. Models of stress changes associated with coseismic slip have been successful in accounting for triggered earthquakes on neighboring faults, and these suggest the importance of stress interactions in controlling the development (i.e., cumulative displacements) of linked fault systems [e.g., *Davison*, 1994]. In this paper we investigate the importance of triggered slip in reactivating preexisting cross faults, faults that are oriented at high angles to the major, basin-bounding normal fault (referred to as a border fault in this paper) in extensional provinces. Although seismogenic triggering of slip along cross faults has been observed most commonly along fault systems with strike-slip motion [*Hudnut et al.*, 1989; *Mori*, 1993; *Ichinose et al.*, 1998; *Smith and Priestley*, 2000], examples in normal faulting environments have also been observed [*Smith et al.*, 2001b] and inferred [e.g., *Janecke*, 1993]. We explore the mechanics and kinematics of cross faults that develop in response to stress changes induced by the growth of a major, basin-bounding normal fault.

[1]Now at Structure, Traps, and Seals Team, Shell International Exploration & Production Inc., Houston, Texas, USA.

0148-0227/03/2002JE001968$09.00

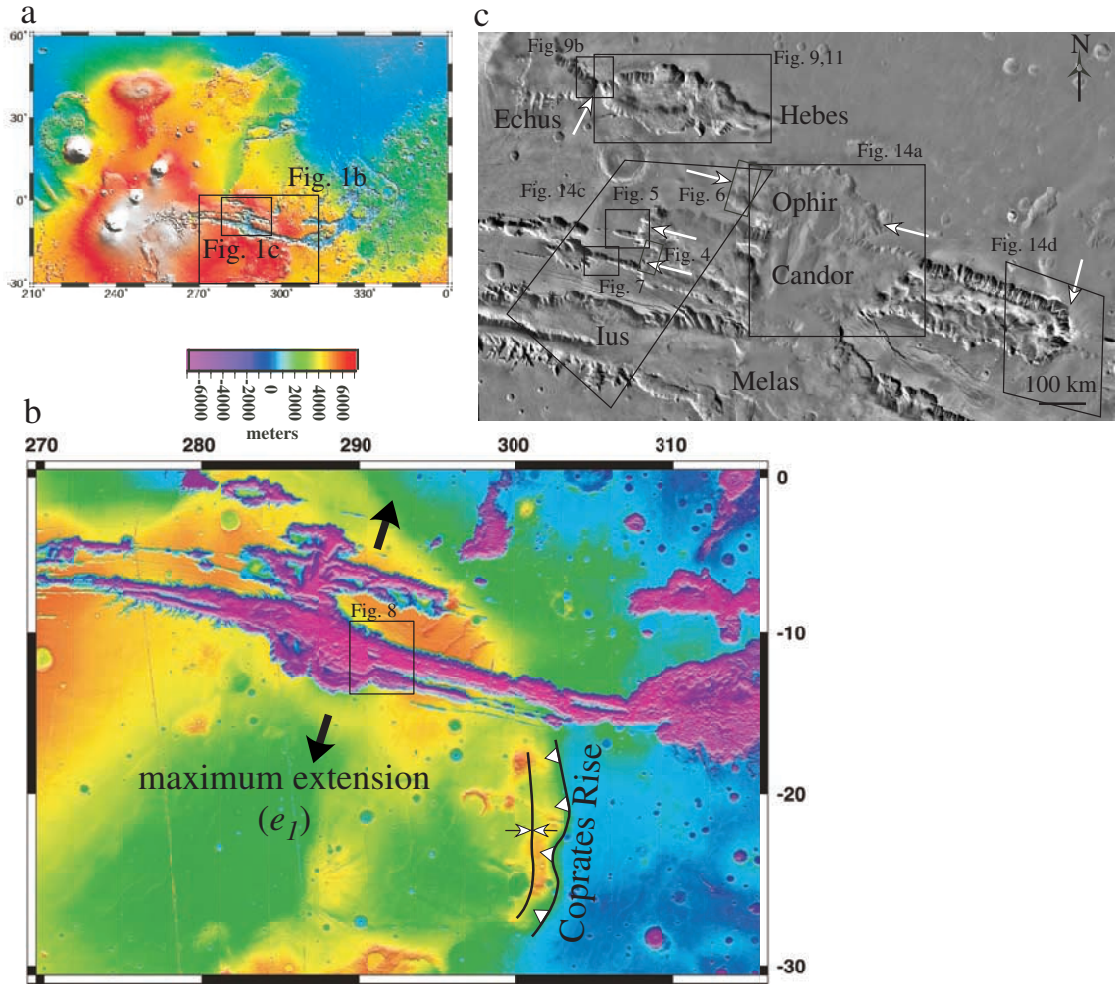

Figure 1. Color-coded topography of (a) Tharsis region derived from MOLA (saturated above 12 km (white), blue is low (∼−8 km); 1/16° spatial resolution; *Zuber et al.* [2000]) and (b) the Coprates quadrangle (MC-18, 125 m/degree, 1° latitude = ∼59 km, scale shown above), which shows the portions of the Thaumasia Plateau (south of Valles Marineris) and interpreted antiform and subsurface thrust fault (teeth point in dip direction) along Coprates Rise [*Schultz and Tanaka*, 1994]. (c) Viking image mosaic of central Valles Marineris. Note the blunt-trough terminations (arrows) at W. Hebes, E. Echus, Candor and Ophir Chasmata.

[3] The motivation for this work stems from conflicting interpretations of rectangular-shaped troughs within the Valles Marineris system of grabens on Mars (Figure 1). Although some researchers have suggested that blunt-ended, rectangular-shaped troughs formed partly in response to erosional processes [e.g., *Spencer and Fanale*, 1990], we explore the possibility that blunt trough terminations are related instead to triggered slip along release faults (defined below), and that a tectonic origin is consistent with observations. We show that irregular troughs, such as Hebes and Candor Chasmata, formed as grabens whose border faults partially reactivated the preexisting cross faults. Our stress transfer modeling provides the first mechanically based explanation that supports faulting for the formation of blunt trough ends within the Valles Marineris extensional province, Mars, and more generally, the locally orthogonal extension observed in numerous extensional environments.

[4] Release faults are a specific class of cross faults that display predominantly normal displacements and are located primarily in the hanging walls of border faults, near the border fault tip line [*Destro*, 1995]. *Destro* [1995] suggested that release faults relieve the bending stress within the hanging wall that arises from along-strike displacement gradients along border faults (Figure 2a). However, cross faults in extended regions have also been referred to as transfer faults [*Gibbs*, 1984, 1990; *Morley et al.*, 1990; *Faulds and Varga*, 1998], after analogies with transfer zones or tear faults in thrust terrains [e.g., *Dahlstrom*, 1969] and transform faults at oceanic spreading centers [e.g., *McKenzie and Morgan*, 1969]. Using fault models that assume constant displacement along the fault surface, *Gibbs* [1984, 1990] argued that strike-slip displacements should predominate along cross faults because they accommodate extension along the main border faults (Figure 2b) (see *Carr* [1981] for application to Valles Marineris).

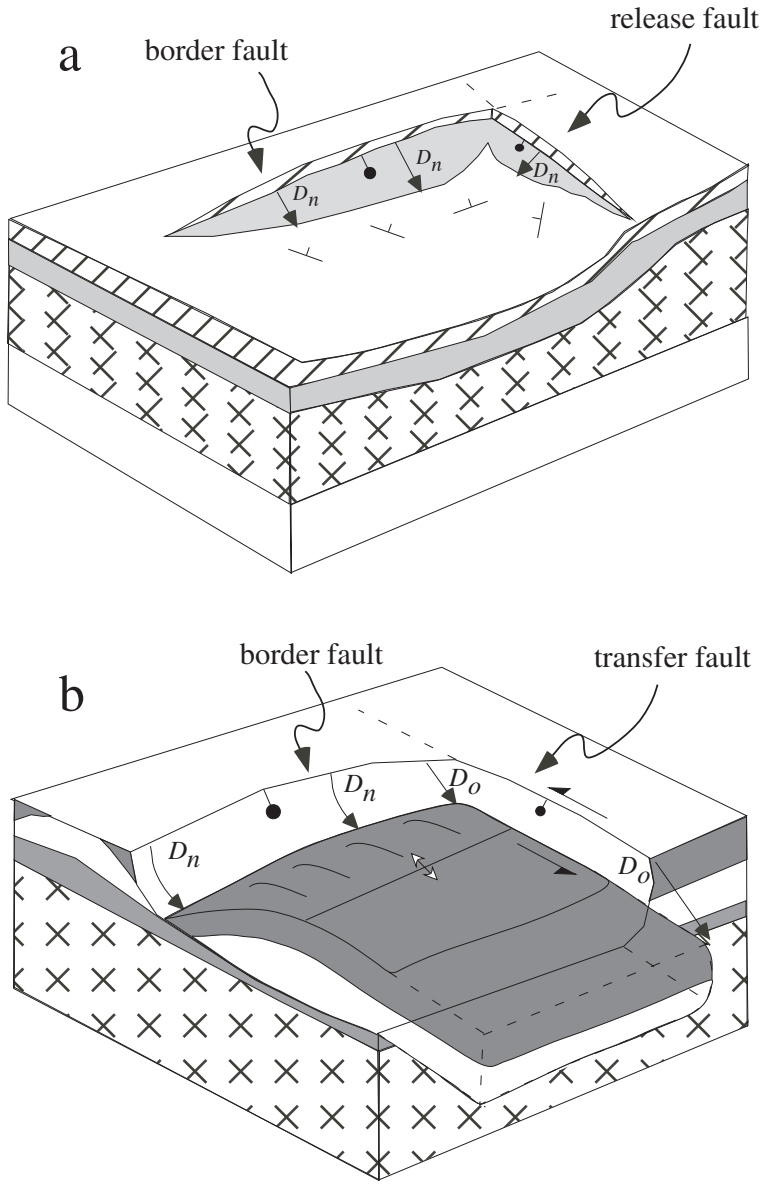

Figure 2. Schematics of the transfer of slip from a border fault to (a) a release fault and (b) a transfer fault (modified from *Destro* [1995] and *Gibbs* [1984]). Pure dip-slip normal displacements (D_n) occur on the release fault, whereas transfer faults accommodate displacements (D_o) that are predominantly strike-slip.

However, mapped cross faults commonly exhibit dip-slip normal or oblique displacements [e.g., *Colleta et al.*, 1988; *Faulds et al.*, 1990; *Janecke*, 1993; *Destro*, 1995; *Roberts and Yielding*, 1994; *Fossen and Hesthammer*, 1998; *Morewood and Roberts*, 2000, 2001; *Maerten et al.*, 1999, 2002], conflicting with *Gibbs'* [1984] model. Furthermore, from detailed structural and stratigraphic work, *Morewood and Roberts* [1997, 2000, 2001] have demonstrated synchronous extension on orthogonal normal faults in terrestrial settings.

[5] Developing a mechanical framework for the evolution of cross faults is important for several reasons. Mechanically based explanations of cross fault development would improve tectonic reconstructions that rely on strain measurements [*Faulds et al.*, 1990; *Morewood and Roberts*, 2001]. For example, we demonstrate that simultaneous normal slip along orthogonal normal faults can occur under a dominantly uniaxial remote plane strain field, which is consistent with conclusions based on geometrical [*Ferrill and Morris*, 2001] and mechanical [*Maerten et al.*, 1999, 2002] considerations. This *local* three-dimensional strain differs from two separate phases of regional extension as sometimes inferred, or from three-dimensional strains that form only if the magnitudes of driving stress do not correspond to plane strain in the slip model of *Reches* [1983] or odd-axis model of *Krantz* [1988].

[6] Second, cross-strike structures commonly occur at the terminus or origin of earthquake ruptures, suggesting they act to limit the along-strike length of coseismic ruptures [*Bruhn et al.*, 1987; *Crone and Haller*, 1991; *dePolo et al.*,

1991; *Janecke*, 1993; *Roberts*, 1996a; *Ichinose et al.*, 1998; *Morewood and Roberts*, 2001]. Rupture length is one of the most important parameters in seismic hazard models [e.g., *Wells and Coppersmith*, 1994] but also one of the most difficult to forecast [*dePolo et al.*, 1991, *McCalpin*, 1996], partly because cross faults (or transverse structures in general) may act as both conservative and non-conservative rupture barriers [e.g., *Roberts*, 1996a].

[7] Third, cross faults have important economic implications in that they may compartmentalize economic deposits [e.g., *Gibbs*, 1990; *Milani and Davison*, 1988; *Morley et al.*, 1990; *Faulds and Varga*, 1998]. Insights about the origin and development of cross faults can provide clues to their spatial extent and structural characteristics, and to previously undiscovered economic reservoirs.

[8] We first provide evidence for cross faults at Valles Marineris, Mars, incorporating geologic interpretations of Viking [*Snyder*, 1977] and Mars Orbiter Camera (MOC) [*Malin et al.*, 1992, 1998] images, in addition to topographic data acquired by the Mars Orbiter Laser Altimeter (MOLA) [*Zuber et al.*, 1992; *Smith et al.*, 1999a]. These observations, together with mechanical models of fault-related topography [*Schultz and Lin*, 2001] and empirically based estimates of slip from earthquake source parameters [*Wells and Coppersmith*, 1994], form the basis for prescribing slip distributions and fault geometries that we use to analyze the slip tendency (i.e., potential for reactivation) of a preexisting cross fault in response to slip on a border fault. Model results are then applied to the general kinematic development of cross faults in extensional settings, as well as the formation of rectangular troughs at Valles Marineris, Mars.

2. Geologic Background of Valles Marineris, Mars

[9] The Valles Marineris are a series of WNW trending, parallel troughs (called "chasmata," defined as elongate depressions) that incise a broad plateau on the eastern flanks of the Tharsis volcanic-tectonic province (Figure 1) [*Sharp*, 1973; *Blasius et al.*, 1977; *Scott and Tanaka*, 1986; *Witbeck et al.*, 1991; *Lucchitta et al.*, 1992]. The uppermost geologic unit on the plateau, the Hesperian-aged ridged plains (Hpl_3 from *Tanaka et al.* [1992]) (Figure 3), is interpreted to represent a regionally extensive series of lava flows [*Scott and Tanaka*, 1986]. Younger deposits exposed within the troughs (i.e., interior layered deposits [*Nedell et al.*, 1987]) span Hesperian through (younger) Amazonian ages, whereas landslide materials are mostly Amazonian [*Witbeck et al.*, 1991; *Lucchitta et al.*, 1992; *Lucchitta*, 1999]. Trough inception began in post-early Hesperian times [*Witbeck et al.*, 1991; *Lucchitta et al.*, 1992; *Schultz*, 1998; *Lucchitta*, 1999]. The Valles Marineris are interpreted here to represent tectonically formed grabens that are bounded by normal faults that dip toward the interiors of the troughs [following *Blasius et al.*, 1977; *Masson*, 1977, 1985; *Lucchitta et al.*, 1992; *Peulvast and Masson*, 1993; *Schultz*, 1998; *Peulvast et al.*, 2001; *Schultz and Lin*, 2001].

[10] The Valles Marineris region includes four major structural elements, listed in their interpreted order of inception, (1) a broad dome [*Tanaka and Davis*, 1988; *Schultz*, 1998] ~4–5 km in height [*Smith et al.*, 1999a], (2)

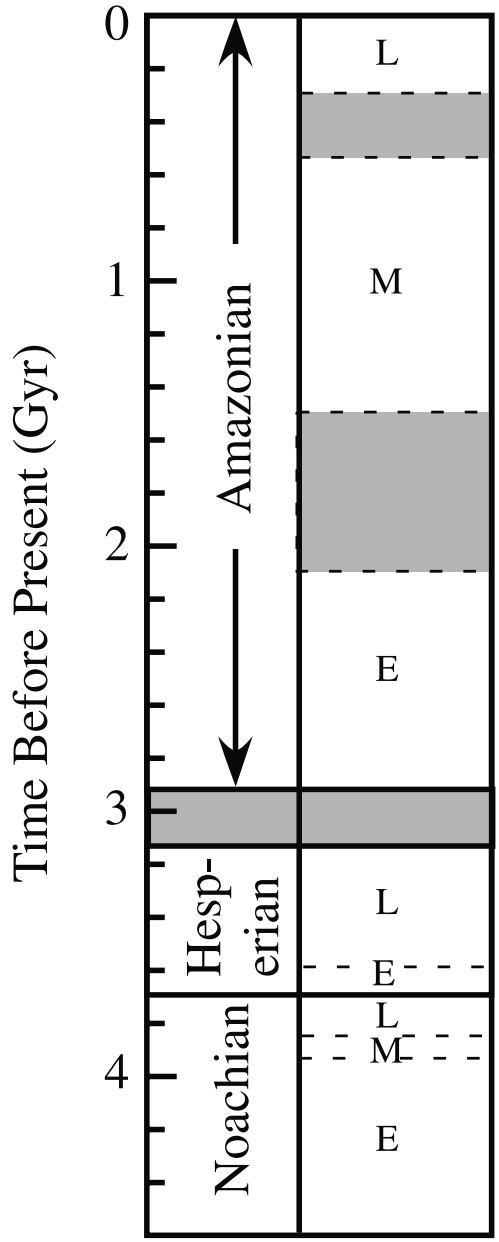

Figure 3. Martian stratigraphic epochs and absolute timescale according to most recent analysis by *Hartmann and Neukum* [2001]. Gray areas show range of possible ages for epoch boundaries. (L) is late, (M) is middle, and (E) is early. Modified from *Zuber* [2000].

~N-S trending wrinkle ridges, interpreted to be anticlines that developed above the tips of blind thrust faults [*Plescia and Golombek*, 1986; *Schultz*, 2000], (3) a widely distributed set of small, ~NNE-SSW trending grabens [*Frey*, 1979; *Witbeck et al.*, 1991], and (4) major ~WNW-ESE trending grabens of Amazonian age that accommodated the maximum component of extension (oriented NNE-SSW) within the region [*Schultz*, 1995; *Mège and Masson*, 1996a]. Numerous, well-exposed fault scarps, aligned *both parallel and highly oblique* to the NNE-SSW axis of extension, displace the youngest material within the troughs (Figures 4–6; Late Amazonian epoch, <~1 Ga)

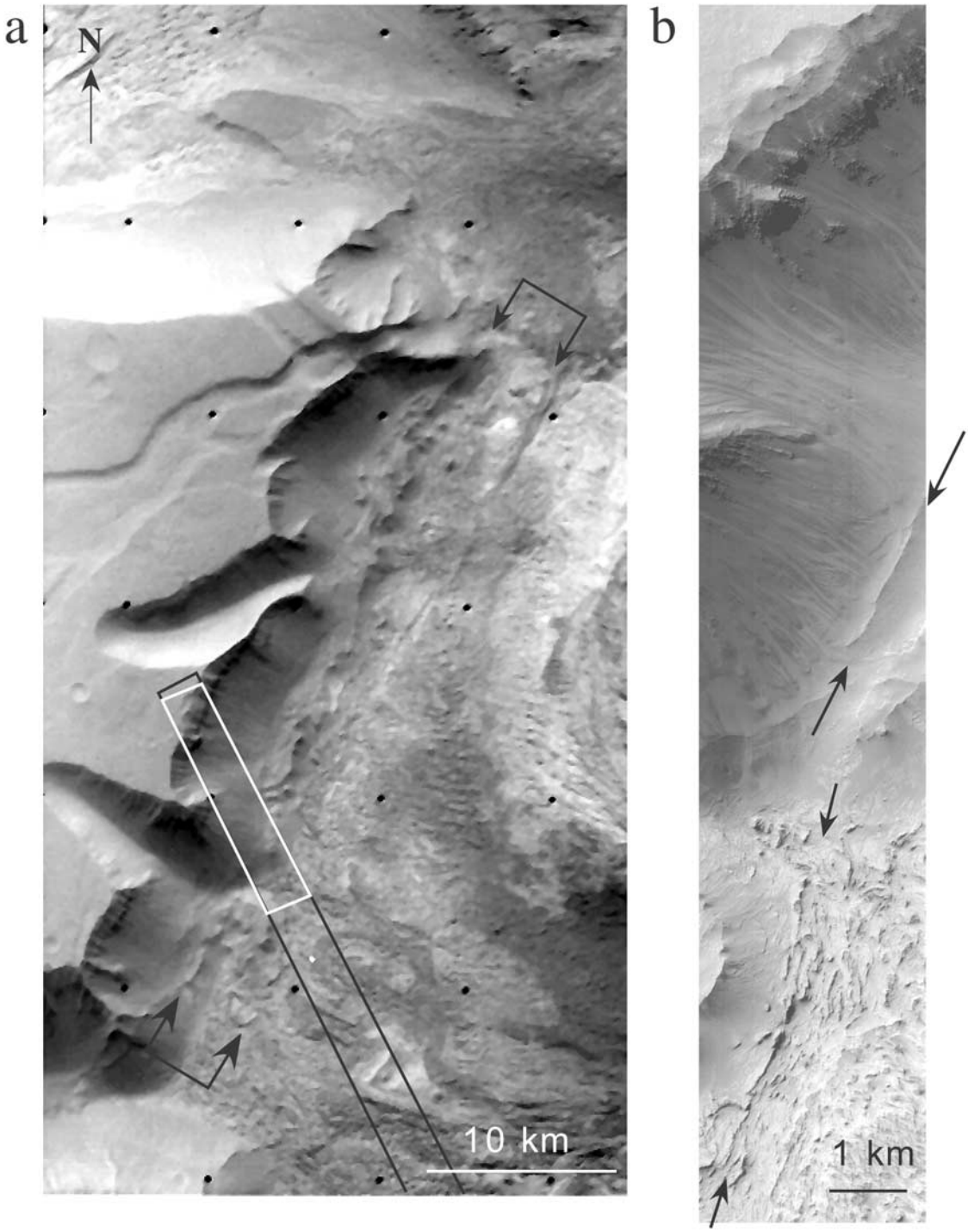

Figure 4. (a) NNE striking fault scarps (i.e., cross-faults, located in zone between arrows) displace landslide deposits derived from the trough walls in Candor Chasma (Viking image 66A20). Mars Orbiter Camera (MOC) image M2101824 location outlined in black, white portion shown in (b). (b) Probable normal fault scarps (between arrows) in Amazonian deposits.

and provide evidence of relatively recent (Late Amazonian) deformation within the troughs [*Blasius et al.*, 1977; *Lucchitta*, 1979, 1999; *Spencer*, 1983; *Schultz*, 1991; *Lucchitta et al.*, 1992]. These observations do not preclude the possibility that both ~N-S striking transverse faults and the main WNW-ESE striking border faults were simultaneously active. On the ridged plains surrounding the troughs, mutually cross-cutting ~N-S and ~E-W trending grabens exist (Figure 7) [see *Witbeck et al.*, 1991], which also suggests coeval growth among these two orthogonal fault sets.

[11] The interpretation of Valles Marineris as an analogue to a terrestrial rift relies on the recognition that the troughs are bounded by normal faults that accommodated extension

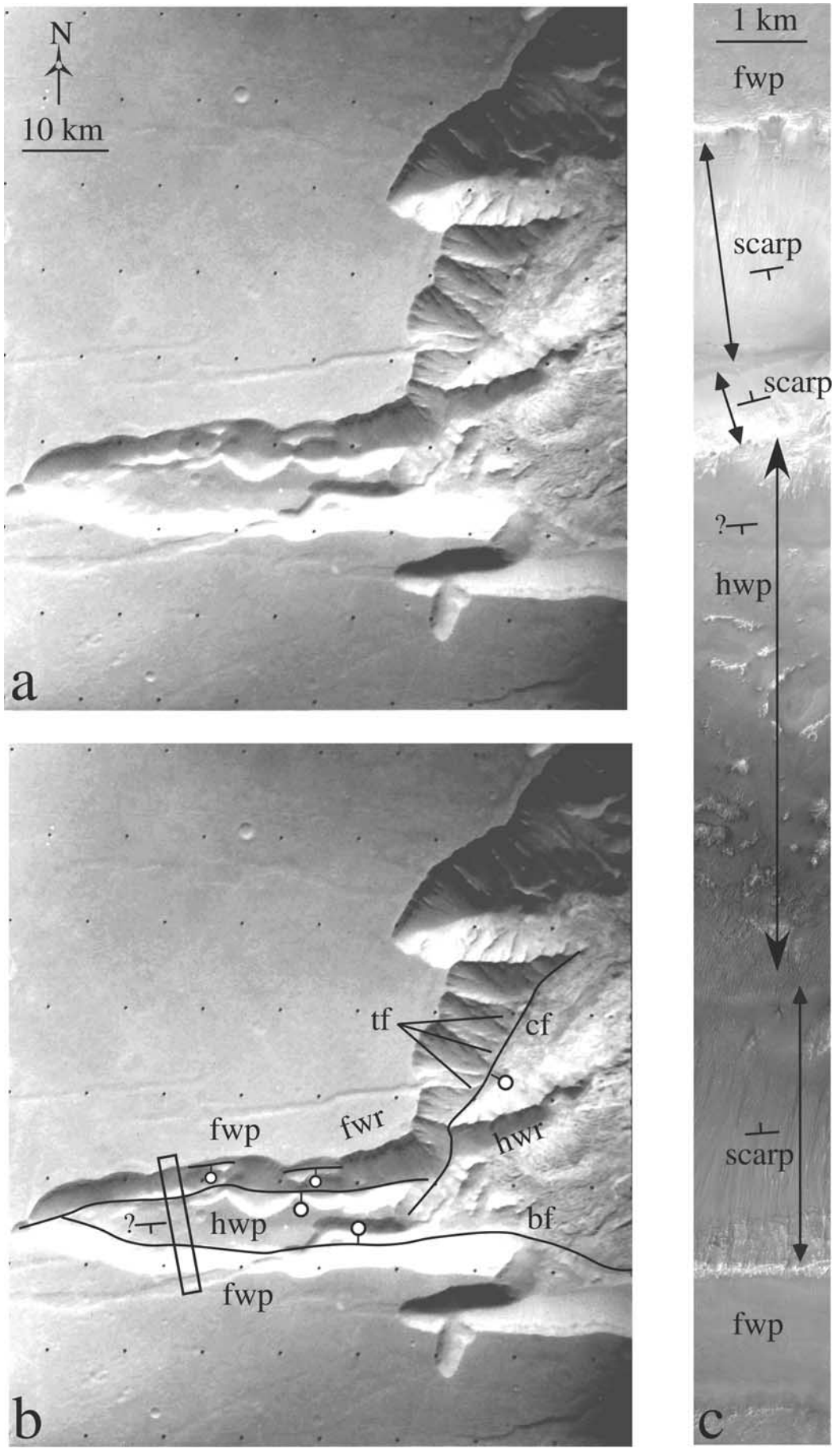
N
10 km
a
tf
cf
fwp
fwr
hwr
?
hwp
bf
fwp
b
1 km
fwp
scarp
scarp
?
hwp
scarp
fwp
c

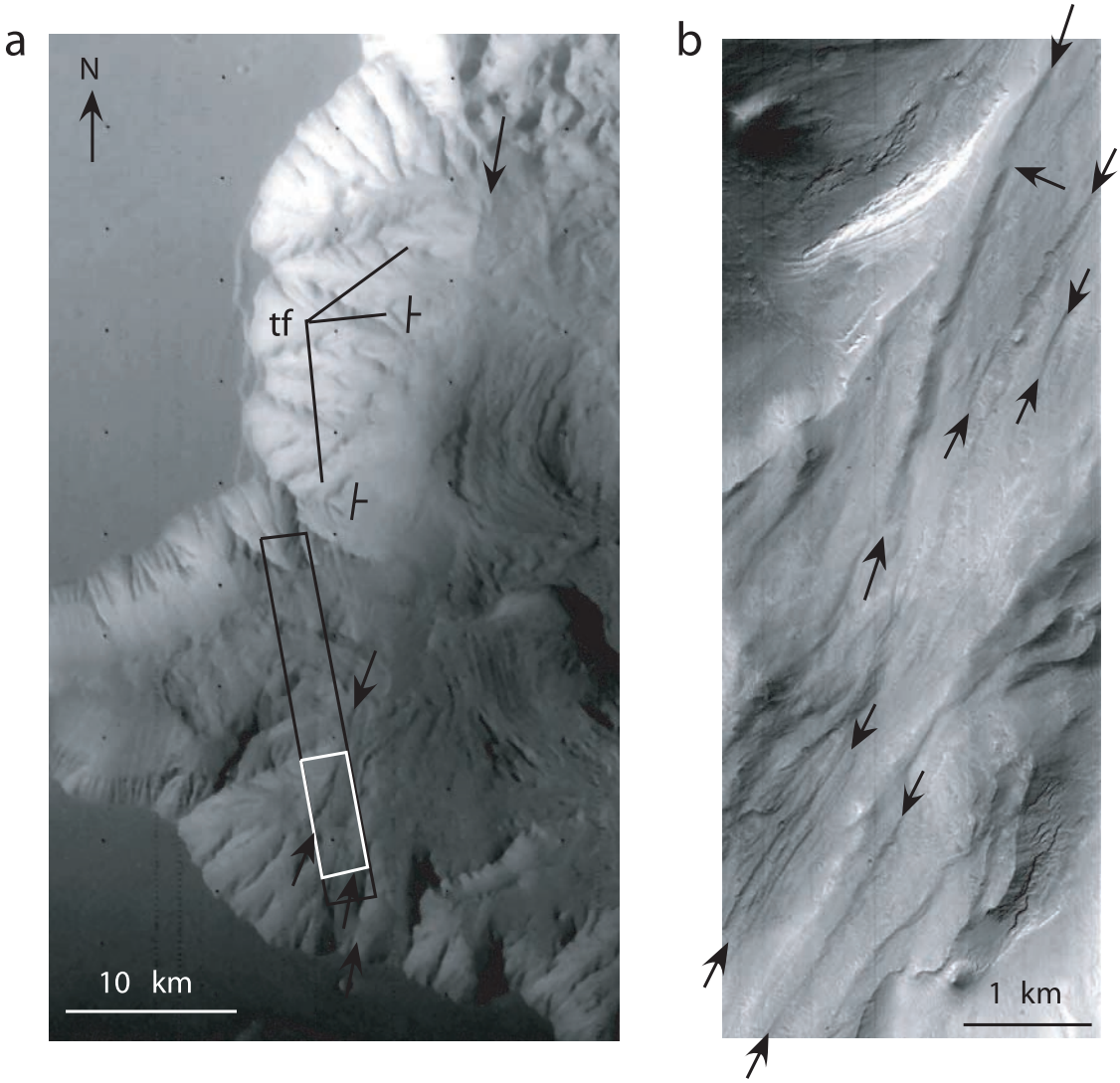

Figure 6. (a) A NNE striking fault is interpreted to breach the surface east of the faceted spurs (dipping east) and hanging gullies on the east facing wall of Ophir Chasma (Viking image 915A10). MOC image M2301765 (5.74 m/pixel) location outlined in black, white portion shown in (b). Triangular facets (tf) are visible on footwall of cross fault. Probable normal cross fault scarps (between arrows) in Amazonian deposits. Note èchelon stepovers along scarps, one example pointed out by northwest trending arrow.

[e.g., *Blasius et al.*, 1977]. Although extensive deposition within the troughs [e.g., *Nedell et al.*, 1987] and erosion of trough walls [e.g., *Lucchitta*, 1979] has obscured some of the evidence for normal faulting [e.g., *Blasius et al.*, 1977; *Schultz*, 1991; *Witbeck et al.*, 1991; *Lucchitta et al.*, 1992; *Peulvast and Masson*, 1993; *Lucchitta*, 1999], morphological evidence of normal faulting is still apparent throughout Valles Marineris. This evidence includes elongate and parallel geometries (Figure 1), linear arrangements of faceted spurs and gullies (Figures 5, 8a, and 9), and basal fault scarps that locally truncate spurs and gullies within the wall rock (Figure 8) [*Blasius et al.*, 1977; *Schultz*, 1991; *Lucchitta et al.*, 1992; *Peulvast et al.*, 2001]. Compelling evidence for the downward displacement of ridged plains plateau materials is given by the presence of plateau materials on trough floors that display the same morphological characteristics and crater densities (i.e., age) as the upland plateau material bounding the troughs (Figure 8) [*Blasius et al.*, 1977; *Schultz*, 1991; *Peulvast and Masson*, 1993; *Lucchitta*, 1999]. Plateau material has been identified on trough floors in Ganges, Capri,

Figure 5. (opposite) (a) Pit-chain emanating from northwest Candor Chasmata (Viking image 065a25, cropped) and interpreted image (b). The cross fault (cf) displaces the hanging wall ridge (hwr) from the footwall ridge (fwr), ball on down-thrown side of fault (solid line). Note the triangular facets (tf) developed at the base of the cross fault scarp where it truncates spur and gully morphology in the footwall. Plateau material in the footwall (fwp) is preserved at a lower structural elevation in the hanging wall (hwp) along the pit-chain, and appears to be tilted southward toward the north facing scarp. Box shows location of (c), MOC image (M14-00191, 2.85 m/pixel).

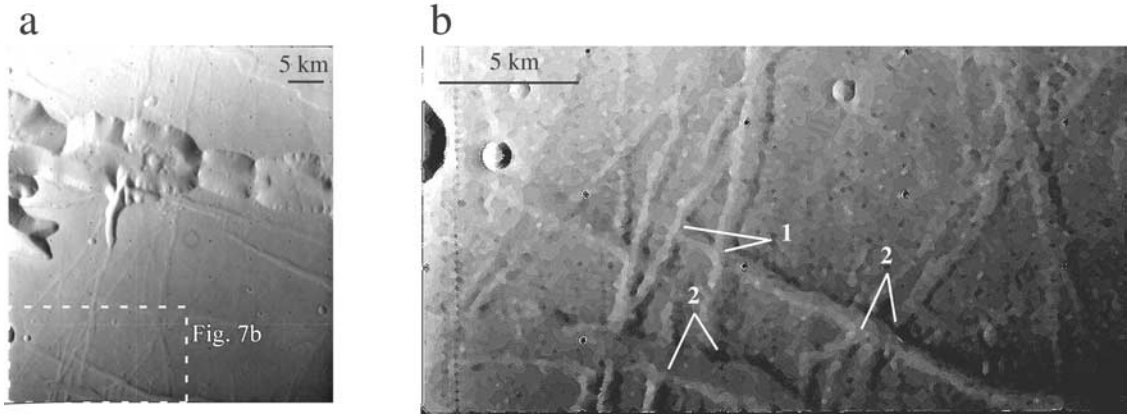

Figure 7. Viking image 919A14 of (a) mutually cross cutting grabens exposed on plateau surface. (b) NNE-SSW trending graben scarps displace WNW-ESE trending grabens at location (1), whereas WNW-ESE trending grabens displace NNE-SSW trending grabens at location (2).

Eos, between Candor and Melas, and Coprates (Figure 8) Chasmata [*Blasius et al.*, 1977; *Schultz*, 1991; *Lucchitta et al.*, 1992; *Peulvast and Masson*, 1993; *Lucchitta*, 1999]. This observation alone does not provide unequivocal evidence for normal faulting because materials could be displaced downward in response to collapse associated with pseudokarst mechanisms [*McCauley et al.*, 1972; *Sharp*, 1973; *Tanaka and MacKinnon*, 2000]; subsurface erosion without the presence of carbonate rocks. However, the apparent continuity of these displaced plateau remnants on trough floors is inconsistent with collapse mechanisms, because chaotically broken and jumbled floors are expected if the rates of downward displacement are sudden (km/sec), in contrast to slower rates associated with faulting (km/Ma) [*Schultz*, 1991]. Furthermore, in some examples the displaced plateau remnant is in contact with a distinct scarp at the base of the trough wall. Such scarps truncate erosional spur and gully morphology within the wall to form triangular facets, and thus provide compelling evidence for normal faults (e.g., Figure 8) [*Blasius et al.*, 1977; *Schultz*, 1991, *Lucchitta et al.*, 1992; *Peulvast and Masson*, 1993; *Peulvast et al.*, 2001].

[12] A passive rifting origin of Valles Marineris has been inferred from the analysis of geophysical data measured with MOLA aboard the Mars Global Surveyor (MGS) satellite [*Smith et al.*, 1999b; *Zuber et al.*, 2000; *Smith et al.*, 2001a]. *Smith et al.* [2001a, pp. 23,609–23,610] stated that "Valles Marineris lacks a regional (topographic) dome. . .which indicates that the canyon system was a consequence of passive rifting [*Sengör and Burke*, 1978] associated with stresses due to the formation of the Tharsis rise, rather than an active rift formed above a localized mantle plume." This interpretation is consistent with the observed negative free-air gravity anomaly (~−400 mGal) that is congruent with the trough topography, and gravity highs along trough flanks (~100–200 mGal), which indicates that the broad negative anomaly commonly found beyond the troughs along active rifts on Earth, does not exist at Valles Marineris [*Smith et al.*, 2001a]. *Anderson and Grimm* [1998] reached similar results on the basis of an analysis of pre-MGS (Viking) gravity and topographic data and suggested that the inferred elastic thickness of the lithosphere (<30 km), low heat flow (>20 mW/m^2), and width of Valles Marineris are consistent with slow, passive rifting.

[13] Similar to terrestrial rift zones associated with lithospheric stretching, the crust beneath Valles Marineris is thinned along its central axis [*Zuber et al.*, 2000]. Furthermore, the Valles Marineris troughs are not isostatically compensated, suggesting the lithosphere has not fully adjusted to their presence [*Smith et al.*, 1999b]. This is consistent with the interpretation that the Valles Marineris formed relatively late (Late Hesperian-Amazonian) in Martian history [e.g., *Schultz*, 1998].

[14] Some researchers have suggested that the Valles Marineris formed in a "transtensive" strain field with both strike-slip and normal displacements along the border faults [*Anguita et al.*, 2001, *Webb and Head*, 2002]. For example, *Anguita et al.* [2001] suggested that Valles Marineris accommodated right oblique motion during the Noachian to Early Hesperian time period [see also *Webb and Head*, 2002]. The inference of right-oblique displacements by *Anguita et al.* [2001] is based on apparent dextral (i.e., right-lateral) offsets of wrinkle ridges on Thaumasia Plateau, along WNW-ESE and ENE-WSW trends, of which the former is similar to the major trend of Valles Marineris troughs. However, right-lateral displacements along Valles Marineris would be inconsistent with east-southeast directed vergence that is thought to be required for kinematic compatibility with the structural development of Coprates Rise during the same general time. Coprates Rise is a north-trending, ~900 km long, east-vergent, asymmetric anticline, interpreted to form in response to folding and thrust faulting by *Schultz and Tanaka* [1994], which may have formed during the same time as the earliest stages of trough formation at Valles Marineris [*Schultz and Tanaka*, 1994]. In contrast to *Anguita et al.* [2001], *Webb and Head* [2002] suggested that Valles Marineris accommodated *left-lateral* displacements in the Noachian to Early Hesperian, in response to gravity-induced sliding of the Thaumasia Plateau toward the southeast (Figure 1b). In their model, left-oblique motion along Valles Marineris is required to be kinematically compatible with east-vergent, contractional structures at Coprates Rise. However, no evidence of strike-slip displacements within or

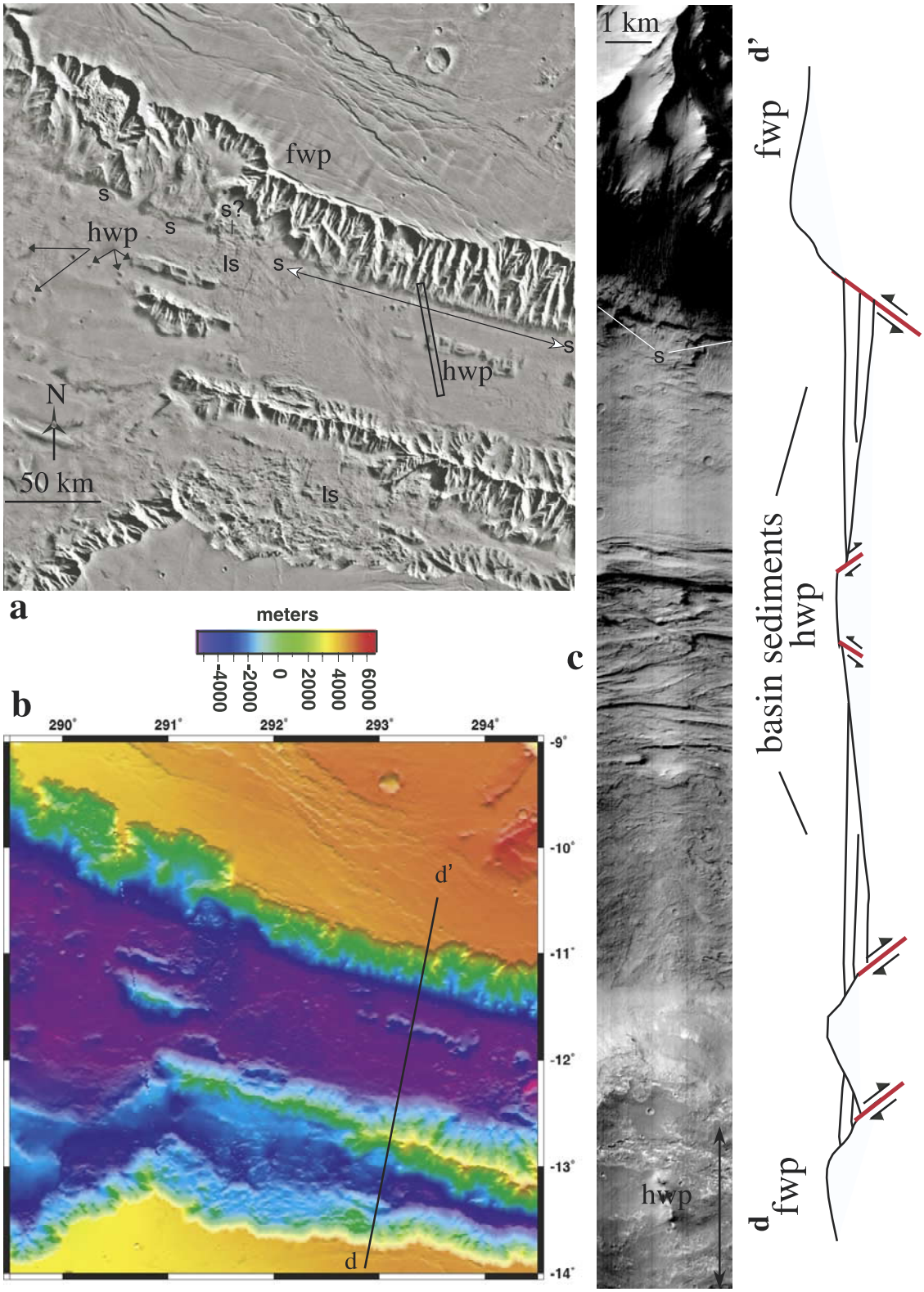

Figure 8. (a) Viking image mosaic (256 m/pixel) and (b) DEM of Coprates Chasma (125 pix/degree, 1° latitude = ~59 km) showing locations of footwall plateau (fwp) and hanging wall plateau (hwp) remnants preserved as mesas on the trough floor. Well-defined, linear basal scarps (s) truncate erosional spurs and gullies on wall rock and appear to truncate landslide materials (ls). (c) MOC image M1902111 (5.68 m/pixel, location shown in (a)) displaying scarp (s) and hanging wall plateau (hwp) remnants. (d-d′) Schematic structural cross section across Coprates Chasma, illustrating an example of how plateau material is exposed in the hanging wall.

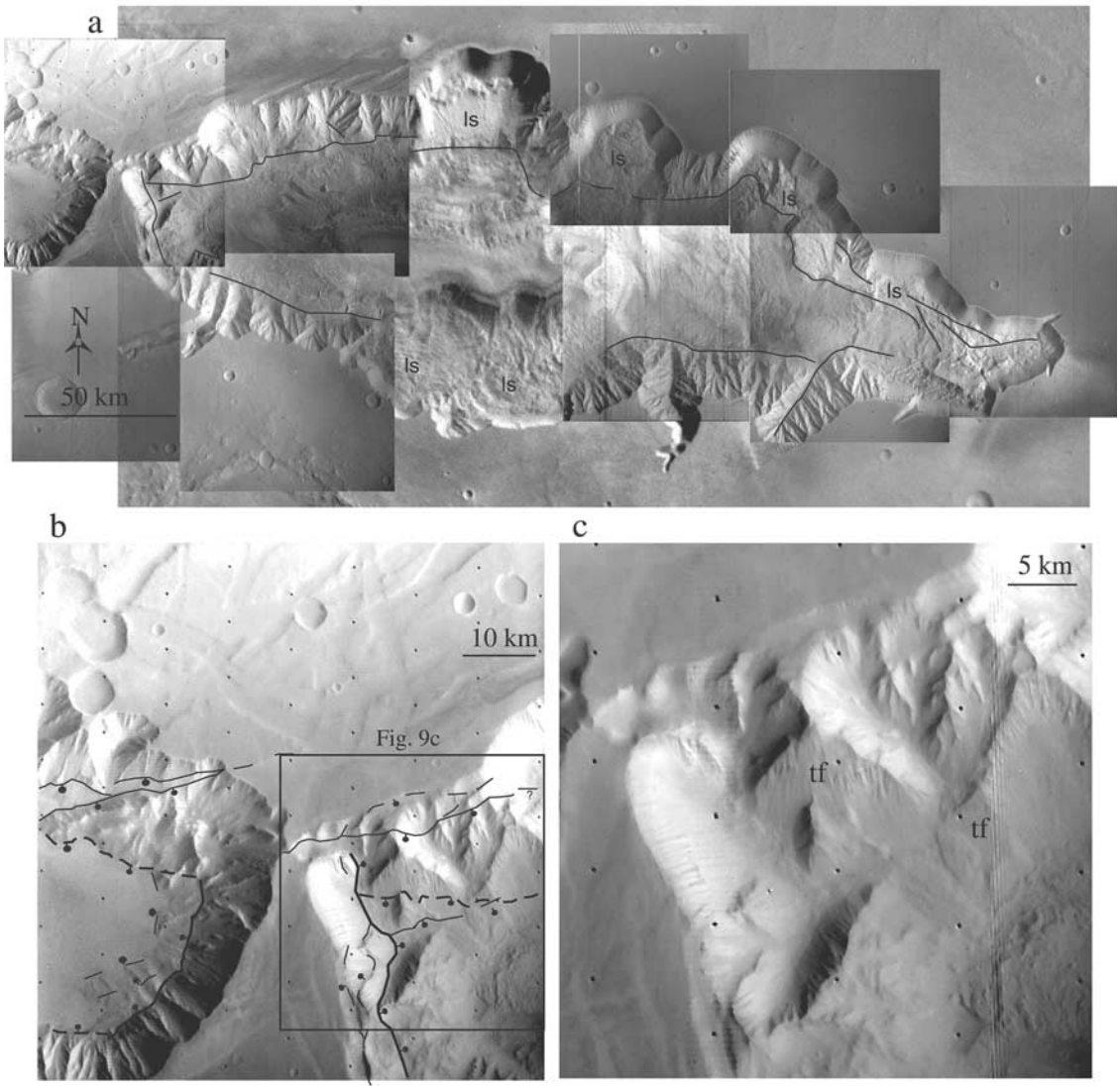

Figure 9. (a) Viking image mosaic (256 m/pixel) of Hebes Chasma, with interpreted faults and landslides (ls). Note the development of spurs and gullies, and triangular facets on trough walls that lack landslide scarps. (b) Viking image (919A04) with major border faults (dashes), cross faults (thick solid lines), and minor border faults (thin solid lines) at NW Hebes and NE Echus Chasmata. Note the orthogonal configuration of the mapped faults. (c) Close-up view of (b). Triagular facets (tf) define the basal fault scarp.

outside the troughs was identified by *Webb and Head* [2002]. Structural or geomorphic evidence for strike-slip faulting may be expected to include 1) laterally offset features such as bedrock, faults (grabens or wrinkle ridges), gullies, ridges or slide deposits; or either 2) pull-apart and/or 3) push-up structures at fault step-overs (i.e., sag-ponds or shutter ridges [*McCalpin*, 1996]; for Martian examples, see *Schultz* [1989]). None of these lines of evidence have been identified in young deposits within the troughs, along basal scarps at the trough walls, or on adjacent plateaus north of the southernmost chasmata [*Blasius et al.*, 1977; *Schultz*, 1991; *Lucchitta et al.*, 1992; *Peulvast and Masson*, 1993; *Lucchitta*, 1999; *Peulvast et al.*, 2001]. Furthermore, structural and stratigraphic relationships suggest that troughs formed after the early Hesperian, [*Witbeck et al.*, 1991; *Lucchitta et al.*, 1992; *Schultz*, 1991; *Lucchitta*, 1999] with the majority of structural displacement having occurred in the Late Hesperian-Early Amazonian [*Schultz*, 1991, 1998]. Trough development therefore primarily postdates any hypothesized episode of strike-slip faulting.

[15] Interestingly, *Purucker et al.* [2000, 2001] interpreted the pattern of magnetic anomalies at Coprates and Ganges Chasmata, Valles Marineris, to have resulted from lateral offsets of ~150 km. However, the structural interpretation is complex because the apparent right-lateral offset of magnetic anomalies at Ganges Chasma and left-lateral offset of magnetic anomalies at Coprates Chasma occur along the same structural trend. This would be difficult to reconcile kinematically or mechanically with the trough geology and tectonics. Additionally, the magnetic anomalies that appear truncated and offset are suspect because they are adjacent to regions of inadequate data coverage [*Purucker et al.*, 2000, 2001]. Furthermore, the interpretation of lateral offsets relies on the assumption that the

magnetization vector is vertical [*Purucker et al.*, 2000, 2001].

[16] Many early researchers favored collapse or erosional processes to explain the development of blunt trough ends at E. Echus, Ophir, Candor, and W. Hebes Chasmata (Figures 1b, 1c, 4–6, 9b, and 9c) because they concluded that tectonic hypotheses are improbable [*McCauley et al.*, 1972; *Carr*, 1981; *Spencer and Fanale*, 1990; *Lucchitta et al.*, 1992]. *Carr* [1981] stated that a normal sense of displacement along trough-bounding cross faults poses a significant problem for tectonic hypotheses. In contrast to the above discussion concerning strike-slip faulting along ENE-WNW striking faults at Valles Marineris, *Carr* [1981] suggested that strike-slip displacements should exist along ~N-S striking faults at blunt trough ends, as required by rigid block fault models (Figure 2b), provided the dominant direction of extension trends ~N-S. The absence of laterally displaced bedrock or geomorphic features at blunt ends of troughs led *Carr* [1981] and subsequent researchers [e.g., *Spencer and Fanale*, 1990] to question a tectonic origin. *Spencer and Fanale* [1990] thus invoked the removal of subsurface carbonate deposits to produce box-shaped troughs. However, in a transect across Hebes Chasma significant carbonate spectral signatures were not observed by the Thermal Emission Spectrometer (TES) [*Christensen et al.*, 1998].

[17] An origin related to collapse is also based on the presence of chains of pit-craters (linear arrays of shallow, scalloped shaped depressions; Figure 5), which are hypothesized to coalesce to form larger chasmata [e.g., *Sharp*, 1973; *Tanaka and Golombek*, 1989]. These chains were explained by stoping into large subsurface voids [e.g., *Sharp*, 1973; *Tanaka and Golombek*, 1989]. Importantly, the formation of voids from subsurface dilatant fractures (i.e., joints or dikes) is not a plausible mechanism for the formation of the large Valles Marineris troughs, because dilatant fracturing should be restricted to the zone of rock mass properties within the uppermost ~2.5 km of the crust, below which shear fractures should form [*Schultz*, 1996, 1998]. In addition, voids produced from subsurface joints or dikes would be too small to accommodate the collapse of the great volume of material necessary to form the troughs [e.g., *Spencer and Fanale*, 1990]. Furthermore, the linearity of pit-crater chains and their association with small grabens and/or perhaps underlying dikes [*Mège and Masson*, 1996b], suggests that subsurface structures controlled the location of secondary erosional or collapse landforms. In some cases, vertically displaced, continuous plateau remnants are exposed in some pit-chains and appear tilted (Figure 5), indicating that these pit-chains may be surface features that formed above subsurface normal faults.

[18] There is no evidence for strike-slip displacements associated with the pit-chains, or features inferred to accommodate lateral displacements (such as échelon chains of faults with depressed ridges at the fault segment step-over, as identified by *Schultz* [1989]), indicating that a comparison with terrestrial sag-ponds is not justified. The lack of spur and gully development on pit-chain slopes provides supporting evidence for relatively recent (Late Amazonian) development, as suggested by *Peulvast et al.* [2001], who suggested that the youngest scarp walls do not exhibit spur and gullied morphologies.

[19] In summary, the greatest problem with previous studies in interpreting the troughs as fault-bounded grabens is the lack of a viable tectonic mechanism capable of forming the blunt ends of the troughs. In this paper, we demonstrate that blunt ends of the troughs may be normal faults, and that dip-slip normal displacements, not strike-slip displacements as suggested by rigid-block models, may have occurred along the cross faults in a dominantly uniaxial, ~N-S extensional regime.

2.1. Fault Geometries and Sequential Development

[20] We first determine the deformation sequence and geometries of cross and border faults to establish a framework necessary for modeling their development. We identify a genetic link between cross faults that form blunt trough terminations and cross faults that exist on the plateau surface. Displacements and surface lengths of border faults are then measured. Using these data, we test the hypothesis that slip on border faults may have triggered reactivation of preexisting cross faults.

[21] Trough-bounding cross faults and faults on the adjacent ridged plains have similar orientations, supporting a possible genetic relationship. To investigate this, we measured the strikes of all cross-strike structures, i.e., wrinkle ridges and normal faults, from a geologic map in the Valles Marineris region [*Witbeck et al.*, 1991]. The normal faults were divided into two groups, those that define the ends of blunt troughs, and shorter structures on the ridged plains (Figure 10). Although wrinkle ridges also exhibit a NNW-SSE strike, ~50% of the wrinkle ridges strike NNE-SSW (average strike of ~14° for n = 52 wrinkle ridges with strikes ranging from 0–52°). Therefore both wrinkle ridges and normal faults on the ridged plains have similar strikes as the trough-bounding cross faults (~NNE-SSW). The similarity in strikes among the major cross faults with both wrinkle ridges and small grabens on the ridged plains supports the possibility that these structures are genetically related. In other words, it is possible that grabens are reactivated wrinkle ridges, or vice versa.

[22] Insights about the sequential development of cross faults can be deduced from the timing of related faults on the plateaus. On the basis of stratigraphic relationships, 1) the wrinkle ridges at Valles Marineris formed prior to the Late Hesperian-Early Amazonian major phase of ~N-S extension [*Frey*, 1979; *Watters and Maxwell*, 1986], most likely during Late Noachian-Late Hesperian times [*Witbeck et al.*, 1991; *Dohm and Tanaka*, 1999] and 2) grabens oriented perpendicular to the main Valles Marineris trend are interpreted to have formed during Late Noachian-Early Hesperian times [*Frey*, 1979; *Dohm and Tanaka*, 1999]. If cross-strike normal faults that define blunt trough terminations originated as older faults associated with wrinkle ridges or small grabens, then the cross faults formed prior to the main phase of Valles Marineris extension. Wrinkle ridges are believed to have formed above subsurface thrust faults [*Plescia and Golombek*, 1986; *Schultz*, 2000]. Such thrusts may have been reactivated as normal faults with a change in the stress field, as demonstrated below. Therefore we infer that blunt trough terminations may either be reactivated normal or thrust faults.

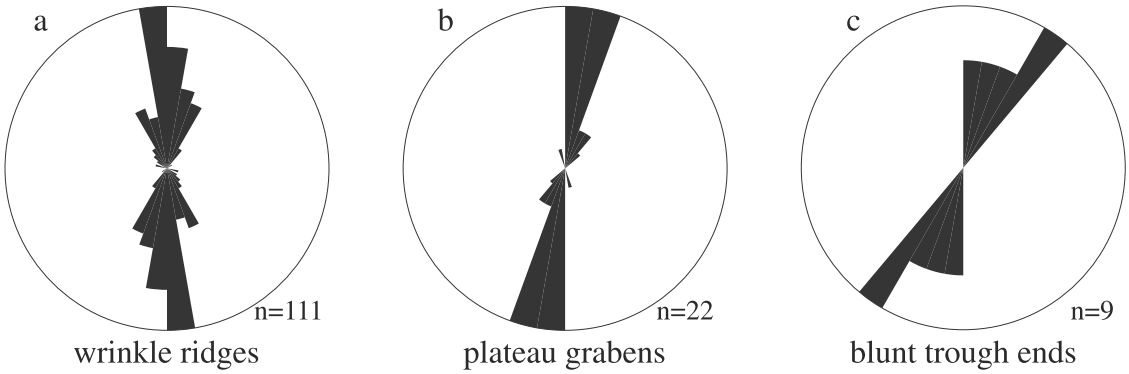

Figure 10. Rose diagrams of strikes of structures on ridged plains surrounding Valles Marineris troughs, including wrinkle ridges (a), grabens (b), and major trough-bounding normal faults at Valles Marineris (c). Mean strikes are 356.4° ± 3.8° (95% confidence interval) in (a), 17° ± 11.3° in (b), and 21.6° ± 8.9° in (c). Note that ~50% of the wrinkle ridges strike east of north, with a mean strike of 14° amongst this group, similar to (b) and (c).

[23] The timing of the major episode of displacement on cross faults is critical to the modeling approach. North-northeast trending fault scarps in the westernmost portions of, for example, Candor (Figure 4) [*Blasius et al.*, 1977] and Ophir (Figure 6) [*Lucchitta*, 1999] Chasmata displace Amazonian-aged deposits within the troughs, attesting to their relatively youthful activity. In the vicinity of Hebes and Echus Chasmata, we mapped ~E-W striking border faults and shorter, ~N-S striking cross faults, both delineated by alignments of faceted spurs and hanging valleys as well as offset ridges of wall rock and erosional surfaces (Figure 9). Mutual cross-cutting relationships exist among grabens that trend ~N-S and ~E-W on the ridged plains plateau (Figure 7) [*Witbeck et al.*, 1991], but cross-cutting relations are not clear among major faults that form the troughs. Nevertheless, evidence of relatively recent slip (i.e., Amazonian), in combination with the inference of prior displacements, suggests the possibility that cross strike structures experienced a multistaged history: an initial phase confined mostly to the Late Noachian-Early Hesperian and extensional reactivation later, during the latest stages (i.e., Amazonian) of Valles Marineris faulting.

2.2. Structural Relief and Fault Segmentation at Hebes Chasma

[24] Hebes Chasma is partly filled with a thick sequence of interior deposits except for a trough adjacent to the wall rock scarp that exposes and reveals the geomorphic evidence of the bounding faults. Geomorphic evidence includes triangular facets and linear scarps with apparent offset of less consolidated and younger materials, relative to the wall rock (e.g., Figure 9). Note that inferred faults with ~N-S strikes are found at both ends of Hebes Chasma, although only the western fault defines the actual trough edge. Displaced Hesperian footwall deposits have not been observed in Hebes Chasma, because they are likely covered by younger interior deposits, similar to grabens on Earth [e.g., *Grosfils et al.*, 2003]. However, footwall deposits have been identified on the trough floors throughout other Valles Marineris troughs (e.g., Figure 8) [*Blassius et al.*, 1977; *Schultz*, 1991; *Lucchitta et al.*, 1992; *Peulvast and Masson*, 1993; *Lucchitta*, 1999]. Thus, as in previous studies on both Earth [e.g., *Cowie and Scholz*, 1992; *Dawers and Anders*, 1995; *Ferrill and Morris*, 2001] and Mars [e.g., *Schultz*, 1991, 1995; *Golombek et al.*, 1996; *Mège and Masson*, 1996a; *Schultz and Lin*, 2001] where the hanging wall is not directly observable, we associate relief along the walls of the trough with minimum structural throw. Inferred structural relief across the northern basin-bounding border fault system within Hebes Chasma (hereafter the N. Hebes Border Fault) is therefore a minimum fault-related throw (i.e., vertical component of displacement, Figure 11). Measurements were made on a digital elevation model (DEM) of Hebes Chasma, based on MOLA data released in December, 2001, with a ~600 m/pixel grid (Figure 11a).

[25] The variation in structural relief along the N. Hebes Border Fault system is similar to displacement variations observed along segmented normal faults (Figure 11c), increasing from minima near the fault tips (i.e., trough ends) and segment boundaries to distinct maximum values in between [e.g., *Anders and Schlische*, 1994; *Dawers and Anders*, 1995; *Morley*, 1999]. Although one of the inferred segment boundaries is overlain by a landslide deposit, the trend of decreasing displacements on both sides of the landslide suggests that a segment boundary exists somewhere within this region.

[26] Previous studies along active terrestrial normal faults have shown that rupture segment boundaries coincide with minima in range heights. For example, along the Wasatch fault zone, Utah [e.g., *Schwartz and Coppersmith*, 1984; *Crone and Haller*, 1991; *Cowie and Scholz*, 1992] and the Dixie Valley-Pleasant Valley normal fault system [*Zhang et al.*, 1991] there exists a correspondence between coseismic slip and cumulative fault displacement patterns, suggesting a general persistence of rupture barriers for some (unknown) portion of the faults history. Interestingly, in these cases the footwall elevation decreases to form displacement minima, whereas at Valles Marineris the hanging wall elevation increases to give displacement minima. The later case is more similar to that observed by *Anders and Schlische* [1994], who show that the footwall decreases in elevation *and* the hanging wall increases in elevation at segment boundaries.

[27] Lengths of the inferred segments at Hebes Chasma are consistent with the upper limit of rupture lengths on

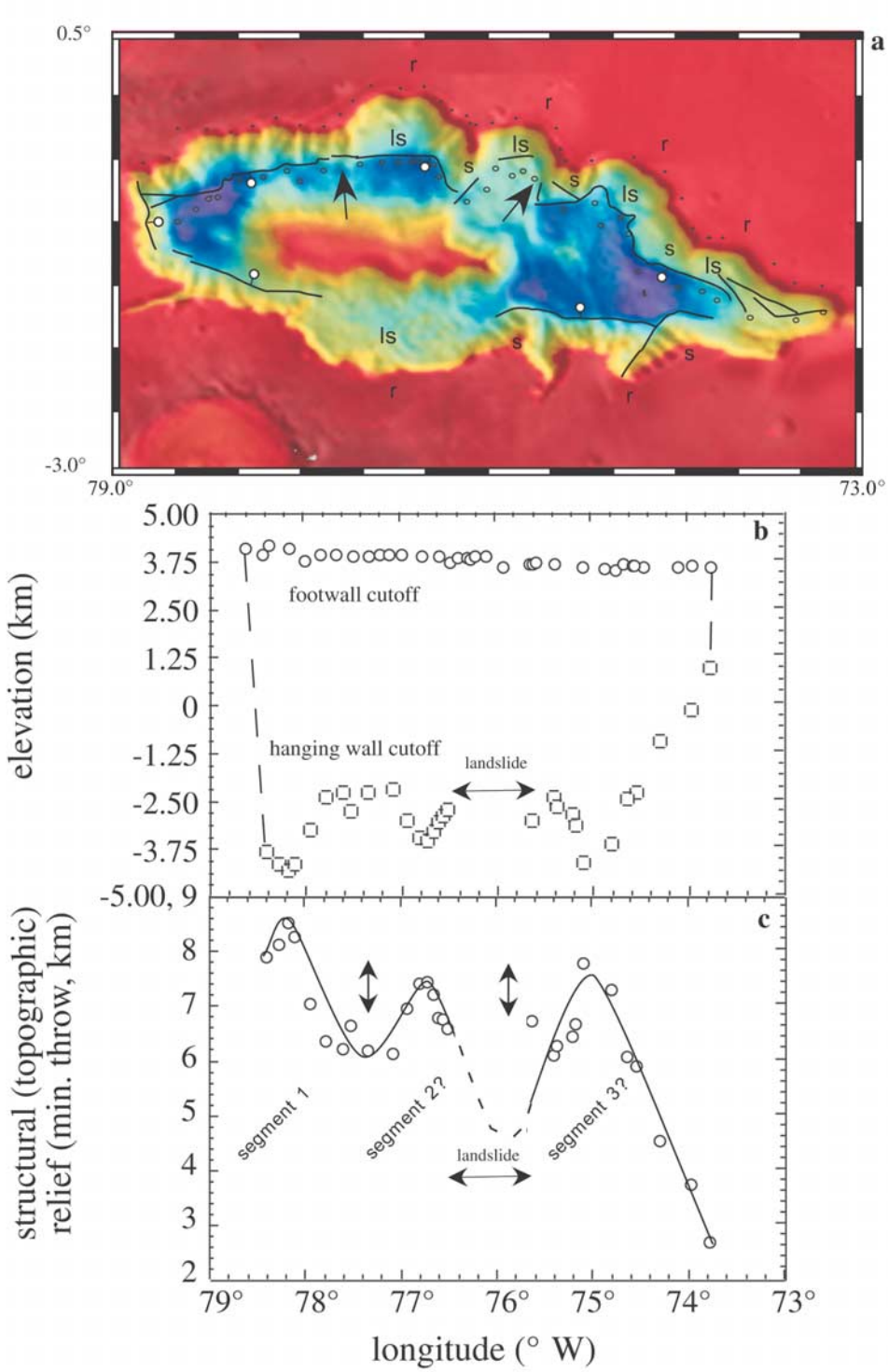

Figure 11. Structural relief across the N. Hebes border fault. Vertical precision of topography measured with MOLA is <∼10 m [*Smith et al.*, 1999a]. Viking topography draped over DEM with locations of measurements on footwall (solid circles) and hanging wall (open circles). Salients (s), reentrants (r), and major landslides (ls) are apparent on the north and south facing walls. Footwall and hanging wall elevations (interpreted as cutoff lines) (b) and structural relief (c). Arrows in image and (c) represent regions of possible segment linkage (1° latitude = ∼59 km). Note the lack of footwall uplift surrounding Hebes Chasma.

normal fault surfaces (~75 km [*Wells and Coppersmith*, 1994]) and maximum lengths of normal faults (~150 km) on Earth [*Scholz and Contreras*, 1998; *Ebinger et al.*, 1999]. Furthermore, the proposed segment boundaries correspond with topographic salients and reentrants, which are commonly associated with rupture barriers on Earth (Figure 11) [*Crone and Haller*, 1991; *Zhang et al.*, 1991; *Janecke*, 1993]. Therefore we use the inferred segment lengths along the N. Hebes Border Fault as the basis for model parameters during fault growth (see section 3.2).

3. Model Description

3.1. Coulomb Failure Stress

[28] We calculate static stress changes to determine whether triggered slip should occur along a preexisting cross fault in response to slip along a perpendicularly oriented normal fault (i.e., border fault). The change in stress resolved along the cross fault is cast in terms of a change in Coulomb failure stress (ΔCFS),

$$\Delta CFS = \Delta\tau - \mu'\Delta\sigma_n \quad (1)$$

where $\Delta\tau$ is the change in shear stress in the slip direction along the cross fault (i.e., rake), μ' is the apparent coefficient of maximum static friction, and $\Delta\sigma_n$ is the change in normal stress (compression positive) on the cross fault [e.g., *King et al.*, 1994; *Harris and Simpson*, 1998]. The apparent coefficient of maximum static friction implicitly accounts for changes in pore pressure that arise from changes in normal stress, bulk moduli and porosity of the fault rock (via Skempton's coefficient for rock B', $\mu' = \mu(1 - B')$ see *Harris* [1998]). We use 0.4, the commonly used value of the apparent friction coefficient [*Harris*, 1998], and note that this value would be compatible with frictional sliding along a border fault with a 50° dip in a regional stress field where the maximum principal stress (σ_1) is vertical ($\sigma_1 = \sigma_v$) and the minimum principal stress (σ_3) is horizontal ($\sigma_3 = \sigma_h$) and perpendicular to the border fault (i.e., N-S strike, see section 3.2). Although changes in pore pressure and dynamic friction during faulting may change μ', modest variations in this parameter would not significantly alter the results [e.g., *King et al.*, 1994; *Schultz and Lin*, 2001]. Stress changes are resolved into ΔCFS along a surface and analyzed using the Coulomb criterion for frictional sliding [e.g., *Jaeger and Cook*, 1979]; a positive ΔCFS value increases the potential for triggered frictional sliding, whereas a negative value of ΔCFS impedes or delays slip. Several studies of aftershock distributions demonstrated that changes in static ΔCFS as low as 0.01 MPa (0.1 bar), or about 1% of average stress drop during an earthquake, are effective in enhancing slip [*King et al.*, 1994; *Harris*, 1998; *Stein*, 1999]; however, *Ziv and Rubin* [2000] found that any positive values may trigger slip. In this study, we interpret positive ΔCFS as a lower threshold necessary for advancing the time to failure and triggering slip along preexisting faults.

[29] We use ΔCFS instead of more sophisticated rate-and-state constitutive failure laws [e.g., *Dieterich*, 1994; *Harris and Simpson*, 1998; *Toda et al.*, 1998]. Rate-and-state formulations incorporate variables not accounted for in the Coulomb frictional sliding criterion, including interseismic sliding speeds (i.e., slip rates), recurrence intervals, and time-dependent fault friction [*Dieterich*, 1994], that are useful in estimating the rate of slip (i.e., stable sliding versus stick-slip). Given the lack of data on temporally dependent changes in slip rate and fault-related friction for Martian faults, we use the simple Coulomb frictional sliding criterion, noting that it is a special case of the rate-and-state formulation [*Gomberg et al.*, 1998]. However, it is important to point out that if stick-slip behavior is dependent on initial stress and state (i.e., effects of contact history among fault surfaces) [e.g., *Dieterich*, 1994] then a simple increase in ΔCFS may not result in an immediate triggering of slip, although it increases the chances for slip in the future [e.g., *Harris and Simpson*, 1998].

[30] Coulomb stress transfer calculations are used to model either incremental stress redistributions associated with coseismic rupture [e.g., *Das and Scholz*, 1981; *King et al.*, 1994], or a greater portion of the seismic cycle by accounting for postseismic deformation [e.g., *Freed and Lin*, 1998] (see review by *Cohen* [1999]). A consequence of a complete seismic cycle is the final slip distribution, which incorporates slip related to both coseismic and postseismic processes. Similarly, cumulative fault displacements are the direct result of multiple seismic cycles, each consisting of both seismic and aseismic fractions of the total deformation. Our primary interest is evaluating the possibility of triggering slip on cross faults in response to a single (coseismic) slip event along a border fault and then assessing the cross fault kinematics if the stress changes are positive.

3.2. Model Approach and Parameters

[31] The procedure we use for calculating ΔCFS involves four steps: (1) determine fault geometries and slip distributions for a range of plausible border fault geometries, (2) solve for the stress field that results from (1) using the three-dimensional boundary element model COULOMB [*King et al.*, 1994; *Toda et al.*, 1998], (3) calculate changes in Coulomb failure stress (ΔCFS) [e.g., *King et al.*, 1994; *Harris*, 1998] resolved onto the cross faults and on along-strike extensions to the border fault to evaluate the possibility of triggered slip, and then (4) determine the sense of motion along the reactivated faults for those portions where Coulomb failure stress is increased sufficiently to promote slip. We analyze a case analogous to the faults of Hebes Chasma, where border fault locations relative to the cross-fault are determined from the image and topographic analyses (section 2.2; Figures 9 and 11). However, the general structural geometry observed at Hebes Chasma is also relevant to many extensional environments on Earth that contain preexisting, cross strike structural features [*Gibbs*, 1984; *Argenton and Maccagni*, 1988; *Colleta et al.*, 1988; *Faulds et al.*, 1990; *Janecke*, 1993; *Destro*, 1995; *Morewood and Roberts*, 1997, 2000, 2001; *Faulds and Varga*, 1998; *Fossen and Hesthammer*, 1998; *Maerten et al.*, 1999; *Poulimenos*, 2000]. We also consider the possibility that (1) lateral propagation of the border fault, along-strike, will be favored instead of reactivation of a preexisting cross fault (Figure 12) and (2) that reactivation of the cross fault may occur in the footwall and/or the hanging wall of the border fault.

[32] Three specific cases (1–3; Figure 12) of boundary fault geometries and slip distributions are specifically tested:

each corresponds to a single slip event along the individual border fault segments observed in Figure 11 and displayed in the model setup (Figure 12b). In each case (1–3), the border faults become progressively longer and farther away from the intersection with the cross fault, consistent with the observations along the N. Hebes border fault. Elliptical slip distributions are prescribed along-strike, with maximum values estimated from empirical relations between surface rupture length (*SRL*) and maximum slip (D_{max}) on terrestrial normal faults ([$\log(D_{max}) = -1.98 + 1.51 * \log(SRL)$] [*Wells and Coppersmith*, 1994, Table 2c]). For each case, we systematically change the dip of the cross fault by increments of 30° to evaluate whether triggered slip can nucleate on preexisting faults with a range of plausible dip angles (A = 30°, B = 60°, C = 90°, Figure 12a).

[33] Geodetic inversions (using COULOMB) based on observed lengths and displacements with solutions that satisfy the relatively small amount of footwall uplift (<0.6 km [*Schultz and Lin*, 2001]) observed with MOLA suggest that the N. Hebes Border Fault dips ~50° to ~60 km depth [*Schultz and Lin*, 2001]. Increasing the fault dip and decreasing the depth both increase the amount of footwall uplift [*Schultz and Lin*, 2001] beyond the observed magnitudes. These results are similar to those obtained for other border faults in Valles Marineris, which suggest faults dip 45–55° to depths of 60–75 km [*Schultz and Lin*, 2001]. In the following models, we incorporate a 50° fault dip to ~60 km depth for the N. Hebes border fault (Figure 12).

[34] Observations and theory indicate that slip vectors may vary as a function of position on faults [*Pollard et al.*, 1993; *Roberts*, 1996b] and possibly result from mechanical interactions with nearby faults [*Cashman and Ellis*, 1994; *Maerten et al.*, 1999, 2002]. Therefore we must evaluate whether slip directions change along the cross faults. To analyze variations in ΔCFS and slip direction as a function of position along the cross fault, cross faults (200 km long) are divided into 40 patches along strike and evaluated at increments of 5 km depth from 0–60 km. Possible lateral propagation of the border fault is also considered. Both ΔCFS and rake along a possible lateral extension (100 km long, 50° dip) of the border fault are analyzed at the same increments as the cross faults (Figure 12).

[35] Local stress changes around faults are spatially variable [e.g., *Pollard and Segall*, 1987; *Ma and Kuznir*, 1993], and therefore we calculate ΔCFS in a three-dimensional half-space, composed of a homogeneous and isotropic linear-elastic material, that accounts for stress changes that arise from free-surface effects [e.g., *Ma and Kuznir*, 1993]. Modeled faults are treated as a planar displacement discontinuity within surrounding homogeneous materials (except for preexisting cross faults and lateral extensions of the border faults). We use a Young's modulus of $E = 60$ GPa and Poisson's ratio $\nu = 0.25$ (Table 1) which is consistent with average elastic properties for basaltic crust on Earth and assumed for Mars [e.g., *Schultz*, 1993, 1996; *Schultz and Lin*, 2001]. The assumed properties represent a simplification of an undoubtedly complex crust with numerous lithological and smaller (than the cross and border faults) structural heterogeneities. However, the simplified model serves as a first-order approximation so that we can begin to understand the general mechanical development of faults at Valles Marineris.

[36] In all calculations, we impose a regional stress field that is appropriate for cohesionless frictional sliding [e.g., *Brace and Kohlstedt*, 1980; *Townend and Zoback*, 2000] along the N. Hebes Border Fault with a dip-slip normal sense of motion. This stress field consists of a vertical σ_1 represented by a depth-dependent overburden load ($\sigma_1 = \sigma_v = \rho g h$; where ρ is density = 2.9 g/cm^3, g is gravity = 3.72 m/s^2, and h = depth), as well as a horizontal σ_3 (= σ_h) oriented perpendicular to the strike of the border fault (i.e., N-S; Figure 7) and that also increases with depth so that the shear stress resolved onto the border fault is constant [e.g., *Townend and Zoback*, 2000]:

$$\sigma_3 = \sigma_1 \left[\left(\mu^2 + 1\right)^{1/2} + \mu \right]^{-2} \tag{2}$$

[*Jaeger and Cook*, 1979; *Engelder*, 1993, pp. 71–75]. The intermediate principal stress ($\sigma_2 = \sigma_H$) is estimated from plane strain boundary conditions in a normal faulting environment, where $\sigma_H = \nu\ (\sigma_v + \sigma_h)$, or $\sigma_2 = \nu\ (\sigma_1 + \sigma_3)$] for normal faults. [*Engelder*, 1993, p. 12]. These conditions are significantly different from those used by *Maerten et al.* [1999], who imposed a depth-independent (constant) σ_v, with uniform horizontal extension (Poissonian expansion) in both the x and y directions. *Bruhn and Schultz* [1996] applied the same regional stress boundary conditions as used here in their study of normal faulting, except they evaluated results in two dimensions and thus did not incorporate an intermediate principal stress (σ_2) parallel to the fault strike.

4. Model Results

[37] Coulomb stress changes along preexisting cross faults and an along-strike, lateral extension of the border fault (LEBF) are displayed in Figure 13. The values of ΔCFS (MPa·10^{-1} = bars) are prescribed for each patch by resolving the induced stress tensor onto frictional surfaces ($\mu' = 0.4$) oriented N-S (i.e., cross fault) and dipping (a) 30°E, (b) 60°E, and (c) 90° and an LEBF (E-W strike, 50°S dip). Slip directions (i.e., rake) are determined from a combination of the induced stress tensor and the regional stress field, where displacement occurs in the direction of the maximum shear stress along the surface onto which stress is resolved.

[38] ΔCFS gradients are generally largest in instances where the border and cross faults intersect (case 1a–c and 2a, Figures 8 and 9). All LEBFs exhibit positive ΔCFS, although the magnitudes significantly decrease away from the tip line of the slipping border fault and as the distance between the slipping border fault and LEBFs increases (from case 1 to 3; Figures 12b and 13). The predicted rake (slip directions of the hanging wall) along the LEBFs are dip-slip normal, similar to the rake along the slipped portion of the border fault (Figure 12).

[39] Moderately dipping cross faults (a–b) exhibit both positive and negative ΔCFS, while negative values dominate for a vertical cross-fault in case 1c and are mostly zero in 2c and 3c. Interestingly, the possibility for triggered slip is decreased along the portion of the cross fault within the border fault footwall only in case 3 (negative ΔCFS), whereas positive ΔCFS occurs in both the border fault

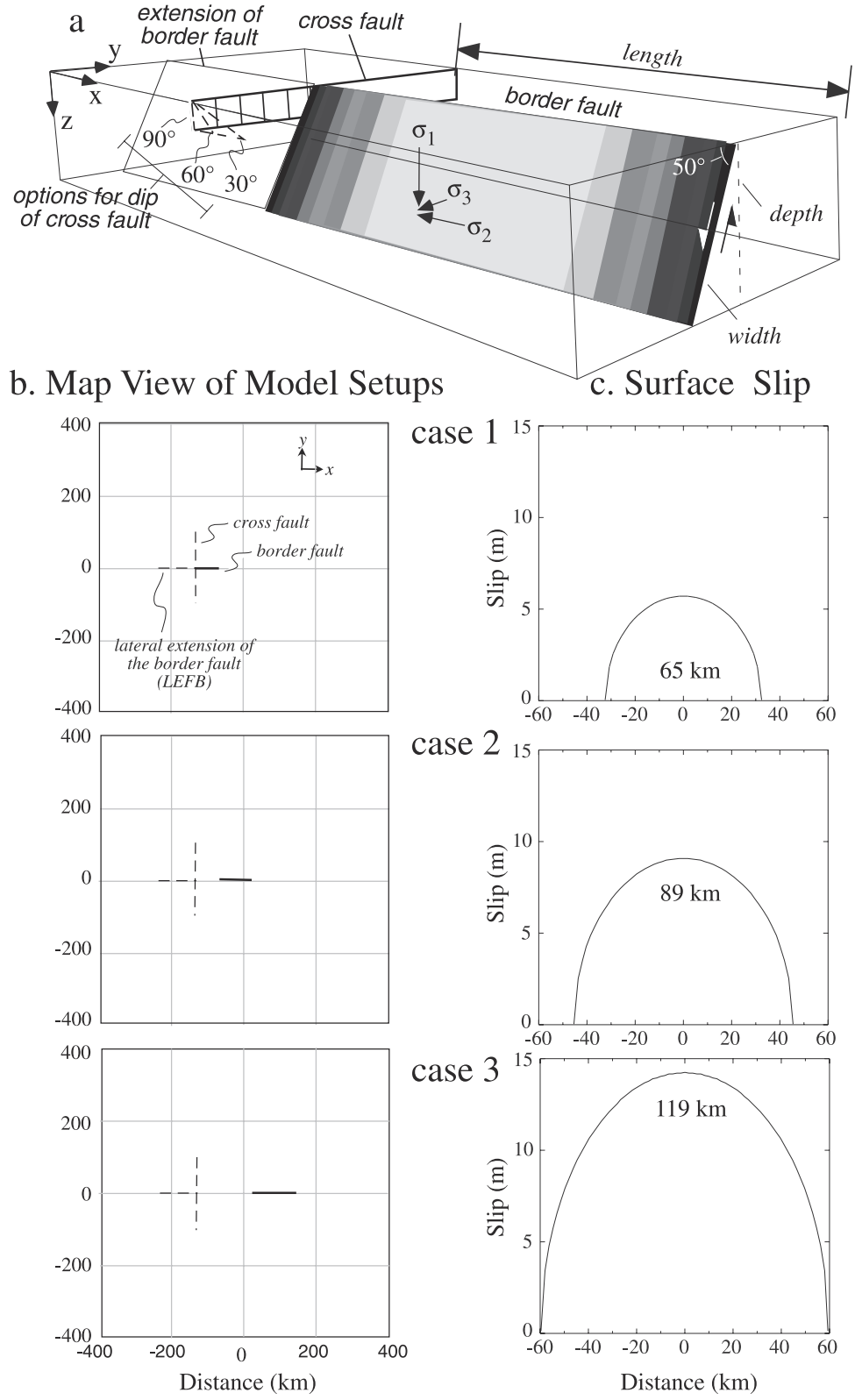

Figure 12. (a) Three-dimensional diagram of model geometries prescribed in COULOMB (not to scale). Schematic contours (shaded) on the border fault represent a tapered slip distribution, while patches on the cross fault show schematically where the average slip directions and stress changes are calculated. (b) Scaled diagram (map view, units are km) of fault geometries during border fault slippage and (c) slip distribution at the surface during each slip event along the border fault.

Table 1. Fault and Material Parameters

Parameter	Value
E, Young's modulus, Gpa	60.0
ν, Poisson's ratio	0.25
ϕ, fault dip	50°
w, depth of faulting, km	60
G, shear modulus = $E/2(1+\nu)$(GPa)	24.0
μ', apparent friction coefficient	0.4

footwall and hanging wall in cases 1 and 2. Except for case 1 where the slipped border fault tip line is immediately adjacent to the LEBF, ΔCFS is generally larger on dipping cross faults than border fault extensions. Positive ΔCFS is located in both the footwall and hanging wall of the border fault in cases 1a–b, although large gradients in ΔCFS are apparent. The large gradients represent instabilities in the boundary element model that occurs at fault intersections (S. Toda, personal communication, 2002). Case 2a exhibits similar effects, with generally positive ΔCFS in the border fault hanging wall and negative ΔCFS in the footwall. The magnitude of negative ΔCFS is reduced in case 2b relative to 2a.

[40] The predicted rakes are all dip-slip normal for moderately dipping cross faults and dominantly lateral (i.e., strike-slip) for vertical cross faults. The sense of motion along the vertical faults in cases 1c and 2c may be generalized as left-lateral in the border fault footwall and right-lateral in the hanging wall, with a region of more variable slip in between, while in case 3c, slip directions are predicted to be right-lateral everywhere.

[41] The modeling results suggest that triggered slip along preexisting cross faults and the LEBFs, into the cross fault footwall, are possible within the range of conditions we tested. However, differences in the location of the slipping border fault with respect to the preexisting faults lead to important differences in the calculated ΔCFS along the preexisting faults. These differences provide useful insight into the systematics of fault development within these regions that may be directly tested from observed fault patterns and from future observations.

5. Discussion

5.1. Lateral Propagation of the Border Faults?

[42] Many of the rectangular troughs at Valles Marineris are bounded by ~N-S striking cross faults and longer ~E-W striking border faults, that all apparently dip toward the interiors of the troughs. However, there are numerous examples of linear geomorphic depressions (i.e., pit-chains) located outside the main troughs, which are aligned with the border faults (Figure 14). We suggest that the aligned chains

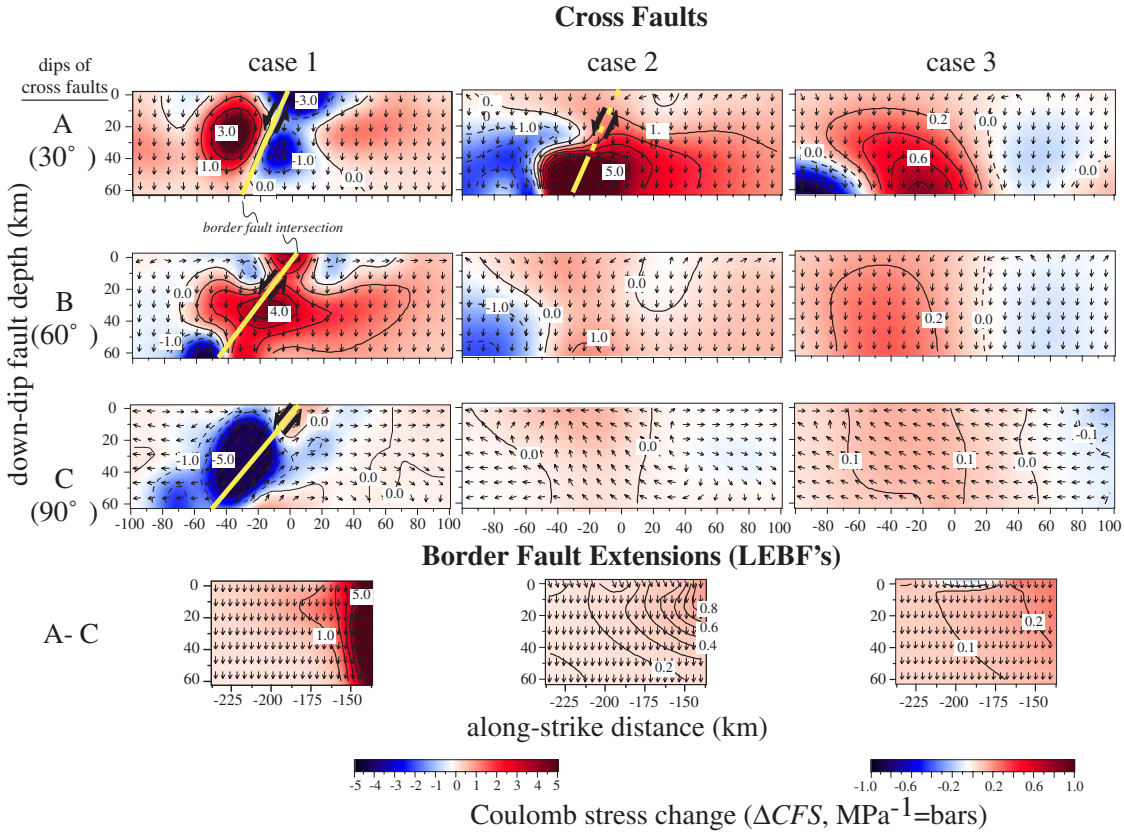

Figure 13. Calculated Coulomb stress changes (ΔCFS) at 0–60 km depth along cross faults and lateral extensions of the border faults (LEBFs). The yellow line represents the intersection of the border and cross fault. Cases 1–3 correspond to geometries of border faults relative to cross faults displayed in Figure 8. Blue represents impeded slip whereas red represents region of potential triggered slip. Arrows represent predicted rake directions.

of pit craters represent relatively recent (relative to border fault development) lateral extensions of the border faults that have less displacement than the faults bounding the troughs. Triggered slip on these LEBFs is predicted to occur in all cases tested (Figure 13), but slip tendency is enhanced when the adjacent border fault tip is closest (case 1).

[43] To determine whether the lateral extensions of the border faults will initiate, we consider the properties of the surrounding rock, which include an assumed average cohesive strength (C_o) of 66 MPa for basaltic rocks (e.g., from the Nevada Test Site basalt, tested within a standard range of confining pressure (3.4–34.5 MPa) [*Goodman*, 1989, p. 83]). Frictional slip will occur when the stress changes equal or exceed the cohesive strength, and follows directly from the relation,

$$\Sigma\Delta\mathrm{CFS} = \Sigma\Delta\tau_i - \Sigma\mu'\Delta\sigma_{n,i} \geq C_o \qquad (3)$$

where i represents each stress change event. Equation (3) assumes that μ' is equivalent for frictional sliding and for the breaking of surrounding rock (i.e., coefficient of internal friction, μ_i). If $\mu_i > \mu'$ [e.g., *Lockner*, 1995], then

$$\Sigma\Delta\mathrm{CFS} = (\tau_r + \Sigma\Delta\tau_i) - \Sigma\mu_i(\sigma_{n,r} + \Delta\sigma_{n,i}) \geq C_o, \qquad (4)$$

where τ_r and $\sigma_{n,r}$ represent the regional shear and normal stress, respectively. If we assume that $\mu_i = \mu'$, then the regional *CFS* ($\tau_r - \mu_i\sigma_{n,r} - C_o$) equals the cohesion, because $\tau_r - \mu_i\sigma_{n,r} = 0$ in the frictional sliding boundary conditions we impose throughout the models. Therefore stress changes related to coseismic stress redistributions must overcome the cohesion for fault nucleation within surrounding rock (equation (3)). If we assume that the border fault has reached its observed length very early during its development [see *Morley*, 1999] so that lateral propagation (and thus increasing fault length) need not be explicitly incorporated in any calculations, we can calculate the magnitude of triggered stress required to propagate the fault. If the average ΔCFS is ~5 bar (case 1), this would require 133 slip events along the border fault to reach the cohesive strength required to fault the surrounding rock. At ~6 m of slip/event, this would accumulate to ~800 m of displacement, which is ~10% of the inferred maximum structural relief (Figure 11). In contrast, if $\mu_i > \mu'$ then more events would be required to nucleate a fault in the surrounding rock mass because the ($\tau_r - \mu_i\sigma_{n,r}$) component is negative in the assumed regional stress field, and therefore larger magnitudes of $\Sigma\Delta\tau_i$ are required for equation (4) to be satisfied. This result would still hold if the (reduced) strength of a rock mass is used [see *Schultz*, 1993, 1996]. These considerations suggest that cross-fault reactivation will be favored initially, while lateral propagation of the border faults, into the footwalls of the cross faults, will occur later in the sequence of fault development. This inference is supported by the observation that LEBFs that lie outside the main troughs of Valles Marineris have smaller displacements (i.e., inferred structural relief; see Figure 14).

5.2. Reactivation of Cross Faults

[44] Coulomb stress change calculations in regions surrounding the border faults predict that triggered dip-slip normal motion will occur along preexisting cross faults, but the model also suggests that significant lateral components of slip are generated in special cases (Figure 13). Specifically, strike-slip reactivation can occur when preexisting fractures are vertical, while dip-slip normal reactivation of the cross faults is predicted to occur for all cases where the faults are not vertical (cases a and b; Figure 13). For the latter cases, we refer to the modeled cross faults as release faults because triggered slip is predominantly dip-slip normal, but note that they may have not initially nucleated to release strain in the hanging wall as envisioned by *Destro* [1995]. In contrast, vertical cross faults (case c) exhibit dominantly lateral (strike-slip) motion except at the fault intersection in case 1, where the displacement is strongly influenced by near-field slip and deformation of the medium around the border fault tip line (Figure 13). In the case of the moderately dipping cross faults, this near-field influence is apparently less important than the regional stress field because the predicted rakes are all dip-slip, even where the faults intersect (case 1a,b and case 2a, Figure 13). The inability of vertical fractures to accommodate normal slip in our models stems directly from the fact that the vertical stress component has no effect on vertical planes, and therefore any increase in shear stress will trigger strike-slip motion.

[45] An important result from our models is the general independence of kinematics and fault dip along a dipping cross fault during triggered reactivation. Triggered slip is characteristically dip-slip (normal) in all tested cases of border fault slip except where cross faults are vertical (Figure 13). Consequently, cross faults can have a variety of different origins (e.g., thrust, reverse, or normal faults) and still be favorably oriented for subsequent dip-slip normal reactivation (Figure 15a). Our model results suggest that cross fault reactivation is favored in the hanging wall of the border fault in case 3, because slip is suppressed in the footwall where stress shadows prevail (Figure 13 and 15 (phase 2b)). In contrast, reactivation of cross faults does not depend on location in cases 1 and 2 (phases 2a, 2b, and 3a in Figure 15), although the ΔCFS is significantly larger near the regions where faults intersect. We thus conclude that reactivation of cross faults may be favored in the border fault hanging wall only where the cross faults are sufficiently distant from the slipping border fault (phase 2b–3b in Figure 15). This indicates that reactivation patterns of cross faults may provide clues to the propagation sequences within extensional environments (see section 5.4).

[46] Furthermore, because cross-faults have similar, and sometimes reduced (but still positive) stress changes relative to LEBFs, we invoke the same mechanical principles described above (section 5.1) to reach the conclusion that cross faults have greater displacements than expected if they *nucleated* in response to border fault slip, rather than simple reactivation of preexisting faults. The latter would require relatively reduced magnitudes of cumulative CFS (i.e., less energy) to drive larger magnitudes of cumulative displacement because the fault surface is already established.

5.3. Development of Release Faults and Implications for Evolution of Cross Faults in Extensional Terranes

[47] Our results suggest that the direction of propagation of border faults has important consequences for displace-

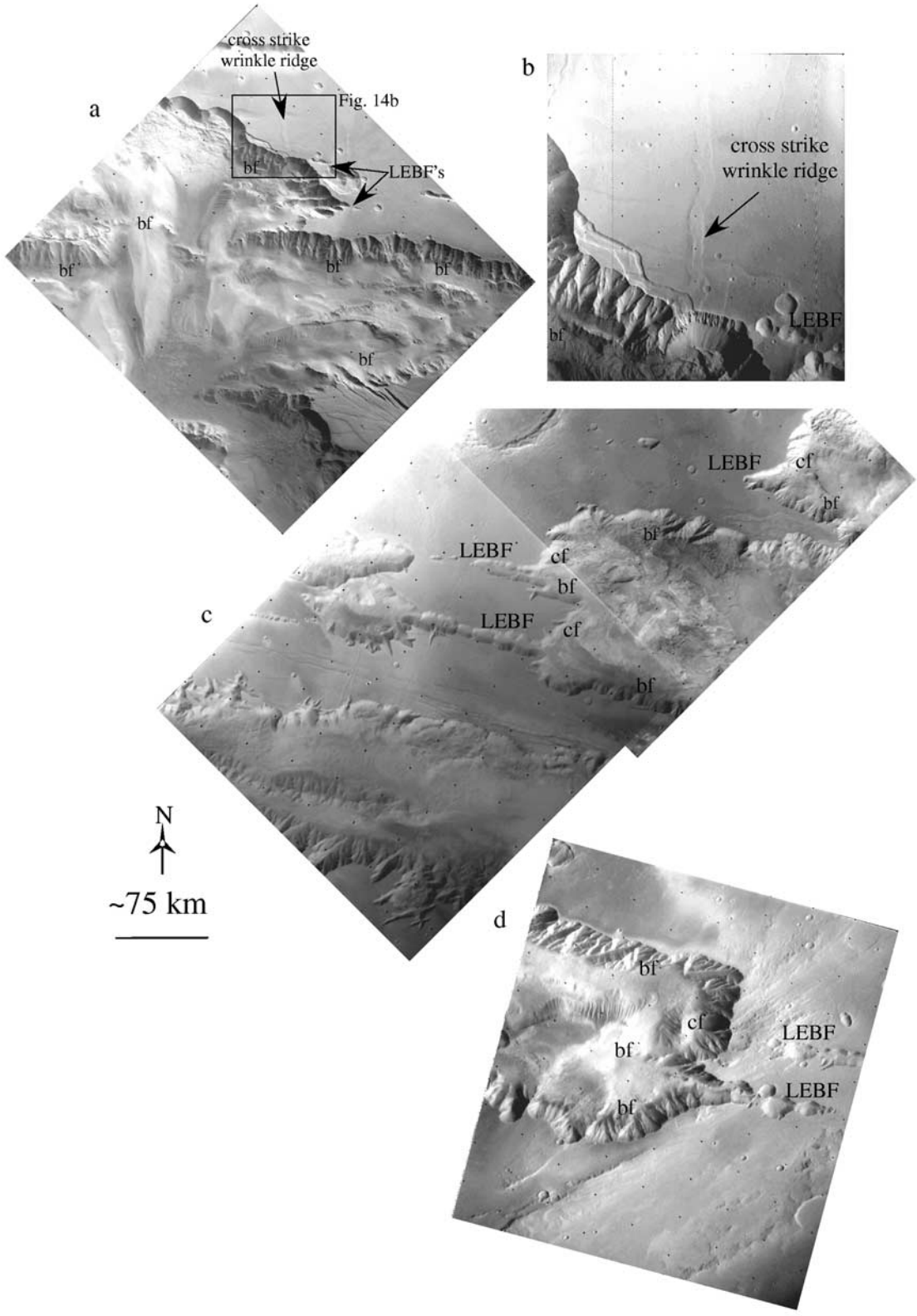

Figure 14. Examples of lateral extensions to border faults (LEBFs) in east Ophir (a,b), west Ophir and Candor (c), and east Candor (d) Chasmata. Cross faults (cf) strike ~N-S and border faults (bf) strike ~E-W throughout Valles Marineris. Note cross-strike wrinkle ridge (a,b) on plateau surface (border fault footwall) that dips to the west (C. Okubo, personal communication, 2002).

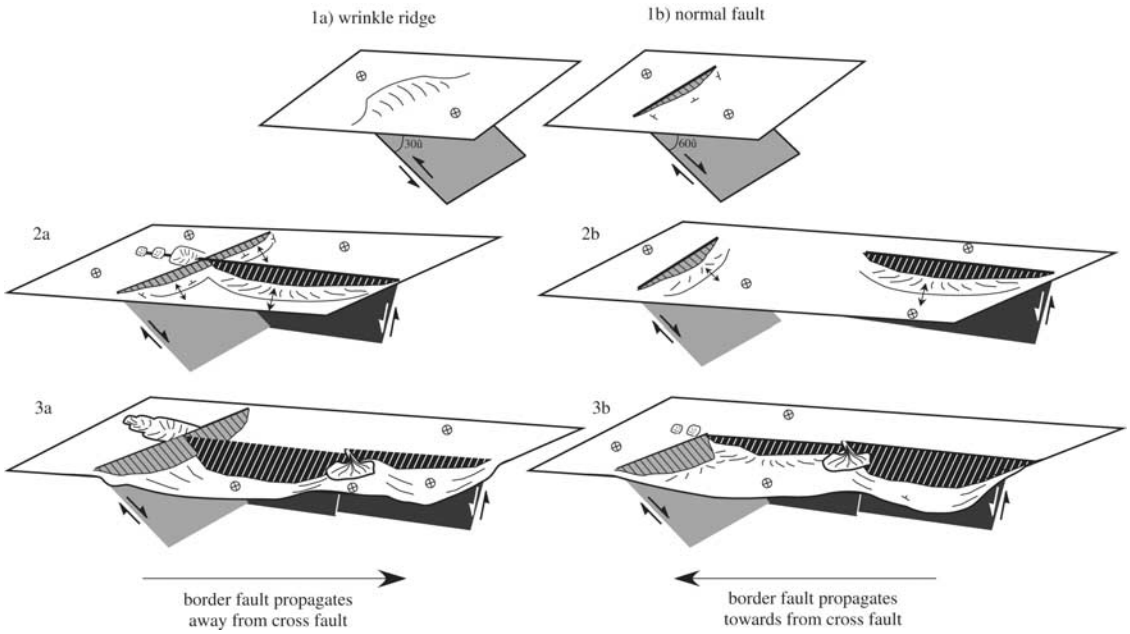

Figure 15. Schematic illustrating two possible sequences of chasma development in response to border fault (black planes) growth and cross fault (gray planes) reactivation. Initial cross faults can be either wrinkle ridges (1a) or normal faults (1b), and subsequent deformation is dependent on the propagation direction of the border faults. When border faults propagate away from cross faults (2–3a), dip-slip normal cross fault reactivation occurs in both the hanging wall and footwall of the border fault and significant development of pit-chains occurs above a subsurface lateral extension of the border fault (within the cross fault footwall). When border faults propagate toward the preexisting cross fault (2–3b), dip-slip normal cross fault reactivation is favored in the footwall of the border fault, and development of pit-chains associated with LEBFs occurs only in the last stage of deformation, once the border fault reaches the cross fault. This latter scenario best matches the observations from many troughs at Valles Marineris.

ment and depositional patterns along cross faults in extensional settings. For example, the absence of troughs within the border fault footwalls (as observed by *Destro* [1995]), suggests that border faults propagated toward the cross fault (phase 2b–3b in Figure 15), whereas the presence of reactivated cross faults in the footwall regions (as observed by *Janecke* [1993]) indicates that the border fault may have propagated away from the intersection with the cross fault (phase 2a–3a in Figure 15). In the latter case, LEBFs should have significant displacements (as observed by *Janecke* [1993]), whereas our models predict that the former scenario would be marked by a young LEBF with little displacement (Figure 14).

[48] *Destro* [1995] suggested that release faults are geometrically required to accommodate variations in displacements along-strike, especially near fault tips where displacement gradients are largest, and thus develop from elongations parallel to the hanging wall and footwall cutoff lines [*Ferrill and Morris*, 2001]. More specifically, *Destro* [1995] suggested that they form to accommodate bending stresses in the hanging wall, which implies that bending stresses do not arise in the footwall. However, numerous authors have presented evidence of uplifted and curved footwall cutoff lines [e.g., *Stein et al.*, 1988; *Ferrill and Morris*, 2001], as are also required by theoretical considerations of footwall uplift along normal faults, whether the uplift results from isostatic restoring forces [e.g., *Weissel and Karner*, 1989] or the elastic response to faulting in the upper crust [e.g., *Pollard and Segall*, 1987; *Ma and Kuznir*, 1993]. The lack of footwall uplift and cutoff curvature (see Figures 11a and 11b) at N. Hebes Chasma may also be an important factor that contributed to the lack of cross fault development in the border fault footwall, because this indicates that a fault-parallel extension may not have developed there.

[49] Considerations of fault growth via segment linkage suggest that large displacement variations may have once existed at former segment boundaries along the border fault [*Dawers and Anders*, 1995; *Morley*, 1999]. In such cases, release faults may be found in more central locations along a subsequently linked fault trace, and may explain similar observations by *Destro* [1995] and *Janecke* [1993].

[50] Late Amazonian normal displacement along the Martian cross faults, as well as along the major border faults, suggests that coeval and nearly orthogonal extension occurred (and is possibly ongoing) within the Valles Marineris extensional province. Coeval and orthogonal extension in our models is a result of reactivation of preexisting cross faults and arises because of *local* perturbations in the stress field. In contrast, the accommodation of a three-dimensional strain by preexisting faults in the slip model of *Reches* [1983] or odd-axis model of *Krantz* [1988] is a result of a regional three-dimensional strain, where the regional stresses do not adhere to plane strain conditions. Coeval and *locally* orthogonal

extension has also been proposed for other extended regions on Earth, such as the Suez rift, Egypt [*Argenton and Maccagni*, 1988; *Colleta et al.*, 1988], Gulf of Corinth, Greece [*Morewood and Roberts*, 1997, 2001; *Poulimenos*, 2000], Sergipe-Alagoas Basin, Brazil [*Destro*, 1995], southern Basin and Range, USA [*Faulds et al.*, 1990], the North-Sea [*Fossen and Hesthammer*, 1998; *Maerten et al.*, 2002], and central Apennines, Italy [*Morewood and Roberts*, 2000]. Our model results and the observations from Valles Marineris troughs suggest that the extension is accommodated with a *local* three-dimensional flattening strain: $e_1 > e_2 > e_3$ where e_1 and e_2 are positive (extension) and e_3 is negative (shortening) [*Ramsay and Huber*, 1983, p. 172; *Morewood and Roberts*, 2000] in a regional, dominantly biaxial strain regime. Regionally, e_1 is positive and trends ~N-S, e_2 is close to zero, and e_3 is negative and vertical (i.e., crustal thinning).

5.4. Origin of Blunt Terminations of Troughs at Valles Marineris

[51] The eastern edge of Hebes Chasma lacks an obvious surficial expression of cross faults, and interestingly, is more tapered in map view than trough edges that are visibly bounded by cross faults (Figures 1c and 9). Because most troughs at Valles Marineris are rectangular (i.e., blunt instead of tapered terminations) and exhibit evidence for cross faults, we infer that the tapered termination of E. Hebes Chasma results from the lack of development of cross faults prior to the major phase of ~N-S extension.

[52] The predominance of normal displacements on cross faults in our model is consistent with the tectonic geomorphology near blunt trough ends within Valles Marineris. Late Amazonian fault activity is apparent near the edges of Hebes Chasma, along both the border faults and the cross faults. Our preliminary mapping also indicates that recent (Amazonian) faulting along cross-strike (~N-S) trends is observable at other blunt trough ends (e.g., W. Ophir, W. Candor; Figures 4 and 6, see index Figures 1b and 1c for full context). The geomorphic evidence for relatively youthful faulting, such as scarps that vertically offset Late Amazonian deposits and linear arrangements of faceted spurs and hanging gullies (Figures 4–6 and 9), is consistent with normal faulting [e.g., *McCalpin*, 1996].

[53] Our model results indicate that reactivation of cross faults to produce normal faults is not sensitive to initial fault dip (except vertical). A direct consequence is that faults associated with earlier stages of wrinkle ridge or normal fault deformation (i.e., pre-Valles Marineris) [*Frey*, 1979; *Watters and Maxwell*, 1986; *Dohm and Tanaka*, 1999] may have been utilized to form cross faults at the blunt terminations of troughs (Figure 15a). Well-developed cross faults do not occur within the footwalls of border faults at Valles Marineris. Therefore pre-Valles Marineris structures were only reactivated to form blunt trough-bounding faults where they intersected the hanging walls of growing border faults. This is consistent with negative ΔCFS (i.e., stress shadows) observed within the footwalls during case 3 of border fault growth, but not cases 1 or 2, suggesting that perhaps the border fault first propagated toward the cross fault (as discussed in section 5.3, (phase 2b–3b in Figure 15). The existence of LEBFs with relatively small trough depths (i.e., vertical structural relief; Figure 14), within the cross fault footwalls and outside of the troughs, provides additional support for this propagation sequence. We would expect larger displacements on LEBFs if slippage commenced on border faults in close proximity to the cross faults (i.e., Case 1 in Figures 8 and 9; phase 2a–3a in Figure 15). This scenario is consistent with the inferred structure at Hebes Chasma (Figure 9). For example, a prominent NNE-SSW striking cross fault occurs ~50 km west of the eastern trough edge at Hebes Chasma (Figure 9). If border faults propagation was toward the west, then the LEBFs would be well developed in eastern Hebes Chasma, as suggested by the extension of the trough toward the east, beyond the cross fault.

[54] Previous researchers suggested that subsurface vertical "tension" fractures [*Tanaka and Golombek*, 1989; *Davis and Golombek*, 1990] or dykes [*McKenzie and Nimmo*, 1999] underlie grabens and led to their formation in Valles Marineris. Evidence for the existence of dykes underneath Valles Marineris include low ratios of displacement to length (but see data and discussion of *Schultz* [1997]), the long length of Valles Marineris, and its apparent spatial association with a large volcano (Pavonis Mons) [*McKenzie and Nimmo*, 1999]. There are numerous problems with *McKenzie and Nimmo*'s [1999] hypothesis, including an incorrect portrayal of the timing of deformation, landslides, and geology within the troughs [see *Schultz*, 1998; *Anderson et al.*, 2001] relative to the timing of possible catastrophic flooding [e.g., *Phillips et al.*, 2001], and the fact that low ratios of fault displacement to length can result for numerous reasons unrelated to dykes (e.g., rock strength, the stage of segment linkage, or degree of restriction). Our results bring to attention another important problem: if cross faults nucleated on vertical fractures, then our models predict that strike-slip displacements should predominate on any associated surface faults. The absence of strike-slip displacements along cross faults suggests that subsurface vertical fractures are not present as large discrete planes in the upper part of Martian crust near Valles Marineris.

[55] New observations from the Mars Global Surveyor and future missions can be used to test our results. Detailed structural mapping of hanging wall deposits and fault-related geomorphology with Mars Orbiter Camera images (highest resolution ~1.5 m [*Malin et al.*, 1992]) should provide useful information on blunt trough terminations. For example, the recognition of cross-strike hanging wall anticlines, such as those interpreted by *Lucchitta et al.* [1992] and *Lucchitta* [1999] in western Ophir and eastern Candor Chasmata, supports the presence of cross-strike normal faults. In contrast, lateral drag folds having vertical fold axes or unfolded strata (i.e., in a vertical sense, with horizontal fold axes) would be indicative of strike-slip faults. Distinct depocenters that commonly occur in the hanging wall of normal fault segments [e.g., *Morley*, 1999] would be relatively small along strike-slip faults, except at extensional step-overs. If the density of the sediment at depocenters is less than the subjacent rock, such depocenters may be detectable from an analysis of gravity measurements once higher spatial resolutions become available [*Zuber et al.*, 2000]. Deployment of seismometers would also aid in delineating these fault-related features near the blunt trough terminations. It would also be useful to analyze and model observed (terrestrial) border fault growth sequences (such as those based on sediment depositional histories [e.g., *Morley*,

1999]) with a finite element model having variable rheologies. Such models should also incorporate propagation and nucleation criteria to develop faults in response to stress changes associated with border fault slippage.

6. Conclusions

[56] Our stress transfer modeling provides the first mechanically based explanation that supports faulting for the formation of blunt trough ends within the Valles Marineris extensional province, Mars, and more generally, the locally orthogonal extension observed in numerous extensional environments. We demonstrate that preexisting normal or thrust faults with strikes parallel to the principal direction of extension in Valles Marineris were locally reactivated with normal slip in response to the growth of border faults to form release faults at blunt trough ends. The lack of significant cross faults in the footwalls of Valles Marineris border faults agrees with model predictions. The match between these observations and model results suggests that border faults grew toward cross faults within Valles Marineris. The result is also consistent with the incipient development of lateral extensions to border faults (i.e., pit-chains overlying subsurface faults) within the footwalls of cross faults.

[57] We provide a new hypothesis for the formation of rectangular, blunt troughs at Valles Marineris: locally concurrent orthogonal extension in the ~N-S and ~E-W directions, that results from *local* stress field changes associated with growth of border faults during predominantly unidirectional regional extension. Our results imply that tapered trough ends formed in areas with no cross fault development prior to the main phase of extension at Valles Marineris. These results are also applicable to many extensional environments on Earth and may be tested with observations of future seismic activity.

[58] **Acknowledgments.** Funding for this project was provided by grants from NASA's Planetary Geology and Geophysics and Mars Data Analysis Programs to R.A. Schultz. S.W. is grateful for discussions with Herb Frey, Steven Cohen, and Coerte Voorhies while visiting at NASA/Goddard Space Flight Center, discussions with S. Toda and R. Stein concerning the boundary element program COULOMB, and reviews by Richard Schweickert and James Faulds. We thank *JGR* reviewers Laurent Maerten, Gerald Roberts, and an anonymous reviewer for insightful reviews that helped us sharpen our thoughts concerning mechanical models of faulting and the development of Valles Marineris.

References

Anders, M. H., and R. W. Schlische, Overlapping faults, intrabasin highs, and the growth of normal faults, *J. Geol.*, *102*, 165–179, 1994.

Anderson, R. C., J. M. Dohm, M. P. Golombek, A. F. C. Haldemann, B. J. Franklin, K. L. Tanaka, J. Lias, and B. Peer, Primary centers and secondary concentrations of tectonic activity through time for the western hemisphere of Mars, *J. Geophys. Res.*, *106*, 20,563–20,585, 2001.

Anderson, S., and R. E. Grimm, Rift processes at Valles Marineris, Mars: Constraints from gravity on necking and rate-dependent strength evolution, *J. Geophys. Res.*, *103*, 11,113–11,124, 1998.

Anguita, F., A.-F. Farelo, V. López, C. Mas, M.-J. Muñoz-Espadas, A. Márquez, and J. Ruiz, Tharsis dome, Mars: New evidence for Noachian-Hesperian thick-skin and Amazonian thin-skin tectonics, *J. Geophys. Res.*, *106*, 7577–7589, 2001.

Argenton, A., and A. Maccagni, Possible axial extension in the Gulf of Suez rift (work hypothesis), *Tectonophysics*, *153*, 297–306, 1988.

Blasius, K. R., J. A. Cutts, J. E. Guest, and H. Masursky, Geology of Valles Marineris: First analysis of imaging from the Viking 1 Orbiter primary mission, *J. Geophys. Res.*, *82*, 4067–4091, 1977.

Brace, W. F., and D. L. Kohlstedt, Limits on lithospheric stress imposed by laboratory experiments, *J. Geophys. Res.*, *85*, 6248–6252, 1980.

Bruhn, R. L., and R. A. Schultz, Geometry and slip distribution in normal fault systems: Implications for mechanics and fault-related hazards, *J. Geophys. Res.*, *101*, 3401–3412, 1996.

Bruhn, R. L., P. R. Gibler, and W. T. Parry, Rupture characteristics of normal faults: An example from the Wasatch fault zone, Utah (USA), in *Continental Extensional Tectonics*, edited by M. P. Coward, J. F. Dewey, and P. L. Hancock, *Geol. Soc. Spec. Publ.*, *28*, 337–353, 1987.

Carr, M. H., *The Surface of Mars*, 232 pp., Yale Univ. Press, New Haven, Conn., 1981.

Cashman, P. H., and M. A. Ellis, Fault interaction may generate multiple slip vectors on a single fault surface, *Geology*, *22*, 1123–1126, 1994.

Christensen, P. R., et al., Results from the Mars Global Surveyor Thermal Emission Spectrometer, *Science*, *279*, 1692–1698, 1998.

Cohen, S. C., Numerical models of crustal deformation in seismic zones, *Adv. Geophys.*, *41*, 133–231, 1999.

Colleta, B., P. Le Quellec, J. Letouzey, and I. Moretti, Longitudinal evolution of the Suez rift structure (Egypt), *Tectonophysics*, *153*, 221–233, 1988.

Cowie, P. A., and C. H. Scholz, Growth of faults by accumulation of seismic slip, *J. Geophys. Res.*, *97*, 11,085–11,095, 1992.

Crone, A. J., and K. M. Haller, Segmentation and the coseismic behavior of Basin and Range normal faults: Examples from east-central Idaho and southwestern Montana, USA, *J. Struct. Geol.*, *13*, 151–164, 1991.

Dahlstrom, C. D. A., Balanced cross sections, *Can. J. Earth. Sci.*, *6*, 743–757, 1969.

Das, S., and C. H. Scholz, Off-fault aftershock clusters caused by shear stress increase?, *Bull. Seismol. Soc. Am.*, *71*, 1669–1675, 1981.

Davis, P. A., and M. P. Golombek, Discontinuities in the shallow Martian crust at Lunae, Syria, and Sinai Plana, *J. Geophys. Res.*, *95*, 14,231–14,238, 1990.

Davison, I., Linked fault systems: Extensional, strike-slip, and contractional, in *Continental Deformation*, edited by P. L. Hancock, pp. 121–142, Pergamon, New York, 1994.

Dawers, N. H., and M. H. Anders, Displacement-length scaling and fault linkage, *J. Struct. Geol.*, *17*, 607–614, 1995.

dePolo, C. M., D. G. Clark, D. B. Slemmons, and A. R. Ramelli, Historical surface faulting in the Basin and Range province, western North America: Implications for fault segmentation, *J. Struct. Geol.*, *13*, 123–136, 1991.

Destro, N., Release fault: A variety of cross fault in linked extensional systems, in the Sergipe-Alagoas Basin, NE Brazil, *J. Struct. Geol.*, *17*, 615–629, 1995.

Dieterich, J., A constitutive law for rate of earthquake production and its application to earthquake clustering, *J. Geophys. Res.*, *99*, 2601–2618, 1994.

Dohm, J. M., and K. L. Tanaka, Geology of the Thaumasia region, Mars: Plateau development, valley origins, and magmatic evolution, *Planet. Space Sci.*, *47*, 411–431, 1999.

Ebinger, C. J., J. A. Jackson, A. N. Foster, and N. J. Hayward, Extensional basin geometry and the elastic lithosphere, *Philos. Trans. R. Soc. London, Ser. A*, *357*, 741–765, 1999.

Engelder, T. E., *Stress Regimes in the Lithosphere*, 457 pp., Princeton Univ. Press, New Haven, Conn., 1993.

Faulds, J. E., and R. Varga, The role of accommodation zones in the regional segmentation of extended terrains, in *Accommodation Zones and Transfer Zones: The Regional Segmentation of the Basin and Range Province*, edited by J. E. Faulds and J. H. Stewart, *Spec. Pap. Geol. Soc. Am.*, *323*, 1–46, 1998.

Faulds, J. E., J. W. Geissman, and C. K. Mawer, Structural development of a major extensional accommodation zone in the Basin and Range Province, northwestern Arizona and southern Nevada: Implications for kinematic models of continental extension, in *Basin and Range Extensional Tectonics Near the Latitude of Las Vegas, Nevada*, edited by B. P. Wernicke, *Mem. Geol. Soc. Am.*, *176*, 37–76, 1990.

Ferrill, D. A., and A. P. Morris, Displacement gradient and deformation in normal fault systems, *J. Struct. Geol.*, *23*, 619–638, 2001.

Fossen, H., and J. Hesthammer, Structural geology of the Gullfaks Field, northern North Sea, in *Structural Geology in Reservoir Characterization*, edited by M. P. Coward, T. S. Daltaban, and H. Johnson, *Geol. Soc. Spec. Publ.*, *127*, 231–261, 1998.

Freed, A. M., and J. Lin, Time-dependent changes in failure stress following thrust earthquakes, *J. Geophys. Res.*, *103*, 24,393–24,409, 1998.

Frey, H., Thaumasia: A fossilized early forming Tharsis uplift, *J. Geophys. Res.*, *84*, 1009–1023, 1979.

Gibbs, A. D., Structural evolution of extensional basin margins, *J. Geol. Soc. London*, *141*, 609–620, 1984.

Gibbs, A. D., Linked fault families in basin formation, *J. Struct. Geol.*, *12*, 795–803, 1990.

Golombek, M. P., K. L. Tanaka, and B. J. Franklin, Extension across Tempe Terra, Mars, from measurements of fault scarp widths and deformed craters, *J. Geophys. Res.*, *101*, 26,119–26,130, 1996.

Gomberg, J., N. M. Beeler, M. L. Blanpied, and P. Bodin, Earthquake triggering by transient and static deformations, *J. Geophys. Res.*, *103*, 24,411–24,426, 1998.

Goodman, R. E., *Introduction to Rock Mechanics*, 2nd ed., 562 pp., John Wiley, New York, 1989.

Grosfils, E. B., R. A. Schultz, and G. Kroeger, Geophysical exploration within northern Devils Lane Graben, Canyonlands National Park, Utah: Implications for sediment thickness and tectonic evolution, *J. Struct. Geol.*, *25*, 24,455–467, 2003.

Harris, R. A., Introduction to special section: Stress triggers, stress shadows, and implications for seismic hazard, *J. Geophys. Res.*, *103*, 24,347–24,358, 1998.

Harris, R. A., and R. W. Simpson, Suppression of large earthquakes by stress shadows: A comparison of Coulomb and rate-and-state failure, *J. Geophys. Res.*, *103*, 24,439–24,451, 1998.

Hartmann, W., and G. Neukum, Cratering chronology and the evolution of Mars, *Space Sci. Rev.*, *96*, 1–30, 2001.

Hudnut, K. W., L. Seeber, and J. Pacheco, Cross-fault triggering in the November 1987 Superstition Hills earthquake sequence, southern California, *Geophys. Res. Lett.*, *16*, 199–202, 1989.

Ichinose, G. A., K. D. Smith, and J. G. Anderson, Moment tensor solutions of the 1994 to 1996 Double Spring Flat, Nevada, earthquake sequence and implications for local tectonic models, *Bull. Seismol. Soc. Am.*, *88*, 1363–1378, 1998.

Jaeger, J. C., and N. G. W. Cook, *Fundamentals of Rock Mechanics*, 3rd ed., 593 pp., Chapman and Hall, New York, 1979.

Janecke, S. U., Structures in segment boundary zones of the Lost River and Lemhi Faults, east central Idaho, *J. Geophys. Res.*, *98*, 16,223–16,238, 1993.

King, G. C. P., R. S. Stein, and J. Lin, Static stress changes and the triggering of earthquakes, *Bull. Seismol. Soc. Am.*, *84*, 935–953, 1994.

Krantz, R. W., Multiple fault sets and three-dimensional strain: Theory and application, *J. Struct. Geol.*, *10*, 225–237, 1988.

Lockner, D. A., Rock failure, in *Rock Physics and Phase Relations: A Handbook of Physical Constants*, *AGU Ref. Shelf*, vol. 3, edited by T. J. Ahrens, pp. 127–147, AGU, 1995.

Lucchitta, B. K., Landslides in Valles Marineris, Mars, *J. Geophys. Res.*, *84*, 8097–8113, 1979.

Lucchitta, B. K., Geologic map of Ophir and Central Candor Chasmata of Mars, scale 1:500,000, *U.S. Geol. Surv. Misc. Invest. Ser. Map, I-2568*, 1999.

Lucchitta, B. K., A. S. McEwen, G. D. Clow, P. E. Geissler, R. B. Singer, R. A. Schultz, and S. W. Squyres, The canyon system of Mars, in *Mars*, edited by H. H. Kieffer et al., pp. 453–492, Univ. of Ariz. Press, Tucson, 1992.

Ma, X. Q., and N. J. Kuznir, Modeling of near-field subsurface displacements for generalized faults and fault arrays, *J. Struct. Geol.*, *15*, 1471–1484, 1993.

Maerten, L., E. J. M. Willemse, D. D. Pollard, and K. Rawnsley, Slip distributions on intersecting normal faults, *J. Struct. Geol.*, *21*, 259–271, 1999.

Maerten, L., P. Gillespie, and D. D. Pollard, Effects of local stress perturbation on secondary fault development, *J. Struct. Geol.*, *24*, 145–153, 2002.

Malin, M. C., G. E. Danielson, A. P. Ingersoll, H. Masursky, J. Veverka, M. A. Ravine, and T. A. Soulanille, Mars Observer camera, *J. Geophys. Res.*, *97*, 7699–7718, 1992.

Malin, M. C., et al., Early views of the Martian surface from the Mars Orbiter Camera of Mars Global Surveyor, *Science*, *279*, 1681–1685, 1998.

Masson, P., Structure pattern analysis of Noctis Labyrinthus-Valles Marineris regions of Mars, *Icarus*, *30*, 49–62, 1977.

Masson, P., Origin and evolution of Valles Marineris region of Mars, *Adv. Space Res.*, *5*, 83–92, 1985.

McCalpin, J. P., (Ed.), *Paleoseismology*, *Int. Geophys. Ser.*, vol. 62, 588 pp., Academic, San Diego, Calif., 1996.

McCauley, J. F., M. H. Carr, J. A. Cutts, W. K. Hartmann, H. Masursky, D. J. Milton, R. P. Sharp, and D. E. Wilhelms, Preliminary Mariner 9 report on the geology of Mars, *Icarus*, *17*, 289–327, 1972.

McKenzie, D. P., and W. J. Morgan, Evolution of triple junctions, *Nature*, *224*, 125–133, 1969.

McKenzie, D. P., and F. Nimmo, The generation of Martian floods by the melting of ground ice above dykes, *Nature*, *397*, 231–233, 1999.

Mège, D., and P. Masson, Amounts of crustal stretching in Valles Marineris, Mars, *Planet. Space Sci.*, *44*, 749–782, 1996a.

Mège, D., and P. Masson, A plume tectonics model for the Tharsis province, Mars, *Planet. Space Sci.*, *44*, 1499–1546, 1996b.

Milani, E. J., and I. Davison, Basement control and transfer tectonics in the Reconcavo-Tucano-Jatob rift, northeast Brazil, *Tectonophysics*, *154*, 41–70, 1988.

Morewood, N. C., and G. P. Roberts, The geometry, kinematics and rates of deformation in a normal fault segment boundary, central Greece, *Geophys. Res. Lett.*, *24*, 3081–3084, 1997.

Morewood, N. C., and G. P. Roberts, The geometry, kinematics and rates of deformation within an en échelon normal fault segment boundary, central Italy, *J. Struct. Geol.*, *22*, 1027–1047, 2000.

Morewood, N. C., and G. P. Roberts, Comparison of surface slip and focal mechanism slip data along normal faults: An example from the eastern Gulf of Corinth, Greece, *J. Struct. Geol.*, *23*, 473–487, 2001.

Mori, J., Fault plane determinations for three small earthquakes along the San Jacinto Fault, California: Search for cross faults, *J. Geophys. Res.*, *98*, 17,711–17,722, 1993.

Morley, C. K., Patterns of displacement along large normal faults: Implications for basin evolution and fault propagation, based on examples from East Africa, *AAPG Bull.*, *83*, 613–634, 1999.

Morley, C. K., R. A. Nelson, T. L. Patton, and S. G. Munn, Transfer zones in the East African rift system and their relevance to hydrocarbon exploration in rifts, *AAPG Bull.*, *74*, 1234–1253, 1990.

Nedell, S. S., S. W. Squyres, and D. W. Anderson, Origin and evolution of the layered deposits in the Valles Marineris, Mars, *Icarus*, *70*, 409–441, 1987.

Peulvast, J. P., and P. L. Masson, Melas Chasma: Morphology and tectonic patterns in Central Valles Marineris (Mars), *Earth Moon Planets*, *61*, 219–248, 1993.

Peulvast, J. P., D. Mege, J. Chiciak, F. Costard, and P. L. Masson, Morphology, evolution and tectonics of Valles Marineris wallslopes (Mars), *Geomorphology*, *37*, 329–352, 2001.

Phillips, R. J., et al., Ancient geodynamics and global-scale hydrology on Mars, *Science*, *287*, 2587–2591, 2001.

Plescia, J. B., and M. P. Golombek, Origin of planetary wrinkle ridges based on the study of terrestrial analogs, *Geol. Soc. Am. Bull.*, *97*, 1289–1299, 1986.

Pollard, D. D., and P. Segall, Theoretical displacements and stresses near fractures in rock; with applications to faults, joints, veins, dikes, and solution surfaces, in *Fracture Mechanics of Rock*, edited by B. K. Atkinson, pp. 277–349, Academic, San Diego, Calif., 1987.

Pollard, D. D., S. D. Saltzer, and A. M. Rubin, Stress inversion methods: Are they based on faulty assumptions?, *J. Struct. Geol.*, *15*, 1045–1054, 1993.

Poulimenos, G., Scaling properties of normal fault populations in the western Corinth Graben, Greece: Implications for fault growth in large strain settings, *J. Struct. Geol.*, *22*, 307–322, 2000.

Purucker, M., D. Ravat, H. Frey, C. Voorhies, T. Sabaka, and M. Acuna, An altitude-normalized magnetic map of Mars and its interpretation, *Geophys. Res. Lett.*, *27*, 2449–2452, 2000.

Purucker, M., B. Langlais, and M. Mandea, Interpretation of a magnetic map of the Valles Marineris region (abstract), *Lunar Planet. Sci.*, *XXXII*, 1865, 2001.

Ramsay, J. G., and M. I. Huber, *The Techniques of Modern Structural Geology*, *Volume 1:Strain Analysis*, 307 pp., Academic, San Diego, Calif., 1983.

Reches, Z., Faulting of rocks in three-dimensional strain fields II. Theoretical analysis, *Tectonophysics*, *95*, 133–156, 1983.

Roberts, A., and G. Yielding, Continental extensional tectonics, in *Continental Deformation*, edited by P. L. Hancock, pp. 223–250, Pergamon, New York, 1994.

Roberts, G. P., Noncharacteristic normal faulting surface ruptures from the Gulf of Corinth, Greece, *J. Geophys. Res.*, *101*, 25,255–25,267, 1996a.

Roberts, G. P., Variation in fault-slip directions along active and segmented normal fault systems, *J. Struct. Geol.*, *18*, 835–845, 1996b.

Scholz, C. H., and J. C. Contreras, Mechanics of continental rift architecture, *Geology*, *26*, 967–970, 1998.

Schultz, R. A., Strike-slip faulting of ridged plains near Valles Marineris, Mars, *Nature*, *341*, 424–426, 1989.

Schultz, R. A., Structural development of Coprates Chasma and western Ophir Planum, Valles Marineris, Mars, *J. Geophys. Res.*, *96*, 22,777–22,792, 1991.

Schultz, R. A., Brittle strength of basaltic rock masses with application to Venus, *J. Geophys. Res.*, *98*, 10,883–10,895, 1993.

Schultz, R. A., Gradients in extension and strain at the Valles Marineris rift, Mars, *Planet. Space Sci.*, *43*, 1561–1566, 1995.

Schultz, R. A., Relative scale and the strength and deformability of rock masses, *J. Struct. Geol.*, *18*, 1139–1149, 1996.

Schultz, R. A., Displacement-length scaling for terrestrial and Martian faults: Implications for Valles Marineris and shallow planetary grabens, *J. Geophys. Res.*, *102*, 12,009–12,015, 1997.

Schultz, R. A., Multiple-process origin of Valles Marineris basins and troughs, Mars, *Planet. Space Sci.*, *46*, 827–834, 1998.

Schultz, R. A., Localization of bedding plane slip and backthrust faults above blind thrust faults: Keys to wrinkle ridge structure, *J. Geophys. Res.*, *105*, 12,035–12,052, 2000.

Schultz, R. A., and J. Lin, 3-D normal faulting models of the Valles Marineris, Mars, and geodynamic implications, *J. Geophys. Res.*, *106*, 16,549–16,566, 2001.

Schultz, R. A., and K. L. Tanaka, Lithospheric-scale buckling and thrust structures on Mars: The Coprates rise and south Tharsis ridge belt, *J. Geophys. Res.*, *99*, 8371–8385, 1994.

Schwartz, D. P., and K. J. Coppersmith, Fault behavior and characteristic earthquakes; examples from the Wasatch and San Andreas fault zones, *J. Geophys. Res.*, *89*, 5681–5698, 1984.

Scott, D. H., and K. L. Tanaka, Geologic map of the western equatorial region of Mars, scale 1:15,000,000, *U.S. Geol. Surv. Misc. Invest. Ser. Map, I-1802-A*, 1986.

Sengör, A. M. C., and K. Burke, Relative timing of rifting and volcanism on Earth and its tectonic implications, *Geophys. Res. Lett.*, *5*, 419–421, 1978.

Sharp, R. P., Mars: Troughed terrain, *J. Geophys. Res.*, *78*, 4063–4072, 1973.

Smith, D. E., et al., The global topography of Mars and implications for surface evolution, *Science*, *284*, 1495–1503, 1999a.

Smith, D. E., W. L. Sjogren, G. L. Tyler, G. Balmino, F. G. Lemoine, and A. S. Konopliv, The gravity field of Mars: Results from Mars Global Surveyor, *Science*, *286*, 94–97, 1999b.

Smith, D. E., et al., Mars orbiter laser altimeter: Experiment summary after the first year of global mapping of Mars, *J. Geophys. Res.*, *106*, 23,689–23,722, 2001a.

Smith, K. D., and K. F. Priestley, Faulting in the 1986 Chalfant, California, sequence: Local tectonics and earthquake source parameters, *Bull. Seismol. Soc. Am.*, *90*, 813–831, 2000.

Smith, K. D., J. N. Brune, D. de Polo, M. K. Savage, R. Anooshehpoor, and A. F. Sheehan, The 1992 Little Skull Mountain earthquake sequence, southern Nevada Test Site, *Bull. Seismol. Soc. Am.*, *91*, 1595–1606, 2001b.

Snyder, C. W., The missions of the Viking orbiters, *J. Geophys. Res.*, *82*, 3971–3983, 1977.

Spencer, J. R., A tectonic geomorphological classification of the walls of Valles Marineris (abstract), in *Reports of Planetary Geology Program*, *NASA Tech. Memo., NASA TM-86246*, 243–245, 1983.

Spencer, J. R., and F. P. Fanale, New models for the origin of Valles Marineris closed depressions, *J. Geophys. Res.*, *95*, 14,301–14,313, 1990.

Stein, R. S., The role of stress transfer in earthquake occurrence, *Nature*, *402*, 605–609, 1999.

Stein, R. S., G. C. King, and J. B. Rundle, The growth of geological structures by repeated earthquakes: 2. Field examples of continental dip-slip faults, *J. Geophys. Res.*, *93*, 13,319–13,331, 1988.

Tanaka, K. L., and P. A. Davis, Tectonic history of the Syria Planum province of Mars, *J. Geophys. Res.*, *93*, 14,893–14,917, 1988.

Tanaka, K. L., and M. P. Golombek, Martian tension fractures and the formation of graben and collapse features at Valles Marineris, Proc. Lunar Planet. Sci. Conf., *19th*, 383–396, 1989.

Tanaka, K. L., and D. J. MacKinnon, Pseudokarst origin for Valles Marineris (abstract), *Lunar Planet. Space Sci.*, *XXXI*, Houston 2000.

Tanaka, K. L., D. H. Scott, and R. Greeley, Global stratigraphy, in *Mars*, edited by H. H. Kieffer et al., pp. 345–382, Univ. of Ariz. Press, Tucson, 1992.

Toda, S., R. S. Stein, R. A. Reasenberg, J. H. Dieterich, and A. Yoshida, Stress transferred by the 1995 Mw = 6.9 Kobe, Japan, shock: Effect on aftershocks and future earthquake probabilities, *J. Geophys. Res.*, *103*, 24,543–24,565, 1998.

Townend, J., and M. D. Zoback, How faulting keeps the crust strong, *Geology*, *28*, 399–402, 2000.

Watters, T. R., and T. A. Maxwell, Orientation, relative age, and extent of the Tharsis plateau ridge system, *J. Geophys. Res.*, *91*, 8113–8125, 1986.

Webb, B. M., and J. W. Head, Noachian tectonics of Syria Planum and the Thaumasia Plateau (abstract), *Lunar Planet. Sci.*, *XXXIII*, 1358, 2002.

Weissel, J. K., and G. D. Karner, Flexural uplift of rift flanks due to mechanical unloading of the lithosphere during extension, *J. Geophys. Res.*, *94*, 13,919–13,950, 1989.

Wells, D. L., and K. J. Coppersmith, New empirical relationships among magnitude, rupture length, rupture width, rupture area, and surface displacement, *Bull. Seismol. Soc. Am.*, *84*, 974–1002, 1994.

Witbeck, N. E., K. L. Tanaka, and D. H. Scott, Geologic map of the Valles Marineris region, Mars, scale 1:2,000,000, *U.S. Geol. Surv. Misc. Invest. Ser. Map*, I-2010, 1991.

Zhang, P., D. B. Slemmons, and F. Mao, Geometric pattern, rupture termination and fault segmentation of the Dixie Valley-Pleasant Valley active normal fault system, Nevada, U.S.A., *J. Struct. Geol.*, *13*, 165–176, 1991.

Ziv, A., and A. M. Rubin, Static stress transfer and earthquake triggering: No lower threshold in sight?, *J. Geophys. Res.*, *105*, 13,631–13,642, 2000.

Zuber, M. T., D. E. Smith, S. C. Solomon, D. O. Muhleman, J. W. Head, J. B. Garvin, J. B. Abshire, and J. L. Bufton, The Mars Observer Laser Altimeter investigation, *J. Geophys. Res.*, *97*, 7781–7797, 1992.

Zuber, M. T., et al., Internal structure and early thermal evolution of Mars from Mars Global Surveyor topography and gravity, *Science*, *287*, 1788–1793, 2000.

R. A. Schultz, Geomechanics-Rock Fracture Group, Department of Geological Sciences, University of Nevada, Reno, NV 89557-0138, USA. (schultz@mines.unr.edu)

S. J. Wilkins, Structure, Traps, and Seals Team, Shell International Exploration & Production Inc., Bellaire Technology Center, P.O. Box 481, Houston, TX 77001-0481, USA. (Scott.Wilkins@Shell.com)